Coordination Chemistry Reviews 253 (2009) 2399–2413

Contents lists available at ScienceDirect

Coordination Chemistry Reviews

journal homepage: www.elsevier.com/locate/ccr

Review

Spin crossover in metallomesogens

A.B. Gaspar[b,**], M. Seredyuk[a], P. Gütlich[a,*]

[a] Institut de Ciència Molecular/Departament de Química Inorgànica, Universitat de València, Edifici de Instituts de Paterna, Apartat de Correus 22085, 46071 València, Spain
[b] Institut für Anorganische und Analytische Chemie, Johannes-Gutenberg-Universität, Staudinger-Weg 9, D-55099 Mainz, Germany

Contents

ARTICLE INFO

Article history:
Received 30 July 2008
Accepted 27 November 2008
Available online 3 December 2008

Dedicated to the memory of Dr. Karlheinz Schmitt.

Keywords:
Spin crossover
Liquid crystal
Phase transitions
Thermochromism
Mesomorphism

ABSTRACT

In this review article are illustrated the strategies developed in order to achieve interplay/synergy between spin transition and liquid crystal transition. The synthesised Fe(II) metallomesogens exhibit different types of interplay between both phase transitions. A classification according to the analysis of the magnetic and structural data has led to the separation of three types of interplay, namely: type i systems with coupled phase transitions, subdivided into three groups *a*, *b* and *c* (in *a* the structural changes associated with the Cr ↔ LC drive the spin transition while in *b* these structural changes influence the spin state of the metallic centers but they are not the driving force of the spin state transition; and *c* concerns the systems where the vitrification of the material inhibits the SCO properties); type ii: systems where both transitions coexist in the same temperature region but are not coupled due to competition with the dehydration; type iii: systems where both transitions occur in different temperature regions and therefore are uncoupled. The synthesised Fe(II) metallomesogens present thermochromism in the room temperature region. By exploiting the fluid nature of these bi-functional materials it is possible to prepare thermochromic thin films of a few μm.

1. Introduction

Metallomesogens are metal-containing-liquid crystals [1]. The first account broadly accepted of these materials dates back to 1910, when the thermotropic properties of alkali metal carboxylates were reported [2]. However, until the late 1970s covalent liquid crystalline coordination complexes were unknown [3]. The study of metallomesogens developed into a very active research field during the last thirty years. The driving force of this research explosion has its origin in the interest to obtain materials combining properties of liquid crystals (fluidity, easy processability, order) with properties associated with metal atoms (magnetism, optics, conductivity, colour) [1]. Future technological demands will require multifunctional materials where several properties of different physical or chemical nature are met in a single material.

The major numbers of metallomesogens reported recently are lanthanidomesogens showing interesting magnetic [4] (paramagnetic liquid crystals, control of molecular orientation in a magnetic

* Corresponding author.
** Co-corresponding author.
E-mail addresses: guetlich@uni-mainz.de (P. Gütlich), ana.b.gaspar@uv.es (A.B. Gaspar).

0010-8545/$ – see front matter © 2008 Elsevier B.V. All rights reserved.
doi:10.1016/j.ccr.2008.11.016

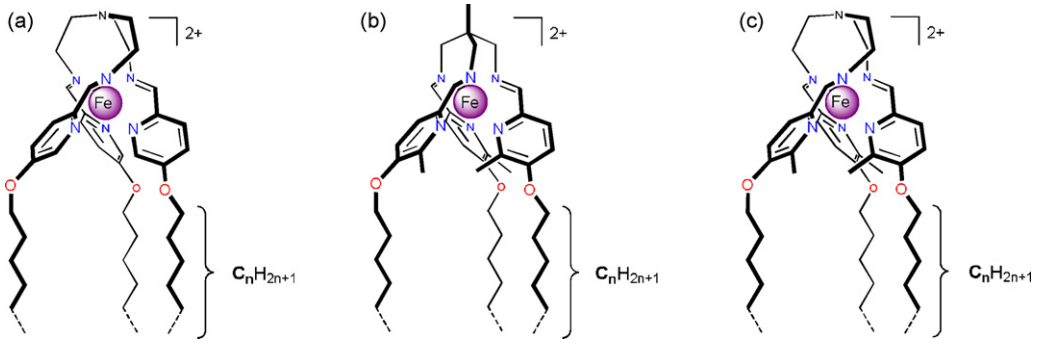

Fig. 1. Schematic structure of complex cations $[Fe(C_n\text{-trenH})]^{2+}$ in **C_n-1** and **C_n-2** (a), $[Fe(C_n\text{-tameMe})]^{2+}$ in **C_n-3** and **C_n-4** (b) and $[Fe(C_n\text{-trenMe})]^{2+}$ in **C_n-7** (c).

field) and occasionally luminescent properties [5]. In fact, metallomesogens exhibiting electrical properties [6] (conductivity), optical [7] (strong birefringence, dichroism, non-linear optical responses) and electro-optical properties (photoelectric behaviour, ferroelectric behaviour) [8], or colour [9] (thermochromism, photochromism) or even redox-active metallomesogens [10] are scarce.

Spin crossover (SCO) materials [11–13] display labile electronic configurations switchable between the high spin (HS) and low spin

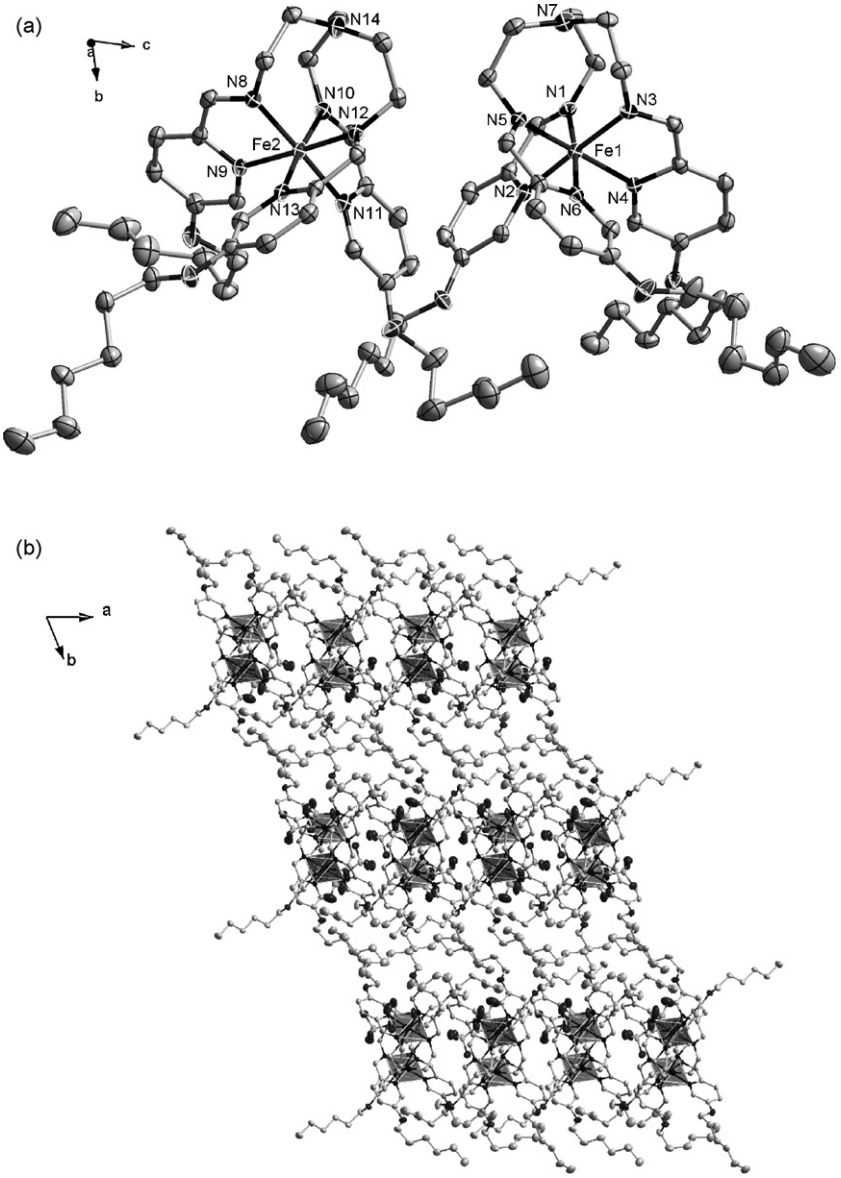

Fig. 2. (a) Projection of the two independent complex molecules of opposite chirality of $[Fe(C_6\text{-trenH})]^{2+}$ contained in the unit cell at 150 K in **C_6-2**. The average Fe(II)–N bonds (1.963(2) Å) and the distortion parameter Σ (67.56(8)°) at 150 K denotes that **C_6-2** is in the LS state. (b) Projection of the molecular packing of **C_6-2** along the *c* axis. Displacement ellipsoids are shown at 50% probability level. Hydrogen atoms and perchlorate anions are omitted for clarity.

(LS) states leading to distinctive changes in magnetism, colour and structure, which may be driven by variation of temperature and/or pressure and by light irradiation (light-induced excited spin state trapping (LIESST) effect) [14]. Their magnetic, optical and structural properties may be altered drastically in a narrow range of temperature and/or pressure for cooperative spin transitions. Cooperativity may be accompanied by hysteresis (memory effect) when the cohesive forces, communicating between the SCO centers in the solid state, propagate the structural changes cooperatively throughout the whole lattice.

A single material combining spin crossover and liquid crystalline behaviour may lead to a number of advantages in practical applications, for example, processing spin crossover materials in the form of thin films, enhancement of spin transition signals, switching and sensing in different temperature regimes, or achievement of photo- and thermochromism in metal-containing-liquid crystals. The change of colour is certainly a phenomenon which is of interest in the field of liquid crystals. The interest lies in the necessity of colour change in a number of applications in liquid crystals such as passive blocking filters, laser addressed devices, polarizers based on dichroic effects, or the utility of thermochromism.

A first step aiming to achieve a material gathering SCO and LC properties has led to an iron(III) metallomesogen where both properties are not synchronous but they appear in different temperature intervals [15]. Later Co(II) and Fe(II) metallomesogens exhibiting similar properties have been synthesised [16,17]. Recently, we have shown that synchronization of spin state and liquid crystal transitions in Fe(II) metallomesogens is achieved by the search for a parent SCO system suitable, after attaching the liquid crystal moiety, to possess LS state or SCO properties at the temperature where the solid–liquid crystal transition is foreseen (275–400 K). Although few examples of Fe(II) metallomesogens have been reported, a very rich interplay/synergy between spin transition and liquid crystal phase transition has been observed: (i) systems with coupled phase transitions, subdivided in three groups *a*, *b* and *c* (in *a* the structural changes associated with the Cr ↔ LC drive the spin transition while in *b* these structural changes influence the spin state of the metallic centers but they are not the driving force of the spin state transition; and *c* concerns the systems where the vitrification of the material inhibits the SCO properties) [18–22], (ii) systems where both transitions coexist in the same temperature region but are not coupled due to competition with the dehydration [18,21–23] and (iii) systems with uncoupled phase transitions [18].

We shall proceed to illustrate the interplay/synergy between spin crossover and liquid crystalline properties in mononuclear and one-dimensional Fe(II) metallomesogens.

2. Fe(II) metallomesogens with coupled spin state and liquid crystal phase transition (type i)

2.1. Type ia: structural changes associated with the Cr ↔ LC drive the spin state transition

Reaction of the ligand tris[3-aza-4-((5-C_n)(6-H)(2-pyridyl))but-3-enyl]amine (C_n-trenH) with $FeCl_2{\cdot}sH_2O$ salts have afforded a family of complexes with general formula [Fe(C_n-trenH)]-$Cl_2{\cdot}0.5H_2O$ (**C_n-1**$\cdot0.5H_2O$) where n = 16, 18 and 20 [18] (Fig. 1a). The analysis of the XPRD patterns at 293 K point out a similar structure as that found for the derivative [Fe(C_6-trenH)]$(ClO_4)_2$ (**C_6-2**). Fig. 2a illustrates the molecular structure of this analogue. The iron atoms adopt a pseudo-octahedral symmetry and are surrounded by six nitrogen atoms belonging to imino groups and pyridines of the trifurcated ligand C_n-trenH. The amphiphilic nature of the alkylated molecules results in the self-assembly to bilayered composite with one layer being made up of polar head groups together with perchlorate anions (Fig. 2b). The non-polar chains from oppositely directed molecules meet together leading to a hydrocarbon layer. Almost fully stretched alkyl chains are only distorted by the *gauche* conformation of some of the methylene groups and tilted toward the *ac* plane but do not intertwine with those of adjacent layers.

The temperature dependent XPRD patterns were recorded following the sequence 310–410–230–410 K and the interlayer distances (d) were derived for derivatives with n = 16, 18 and 20. The temperature variation of d presents an abrupt increase as a consequence of the melting between 340 and 350 K for **C_{16}-1**$\cdot0.5H_2O$ (Fig. 3a). For derivatives with n = 16, 18 and 20 the melting was found at 287, 301 and 330 K, respectively (Table 1). The temperature of melting was further confirmed by differential scanning calorimetry (DSC) and polarizing optical microscopy (POM). On the basis of these observations for these compounds at high temperatures a

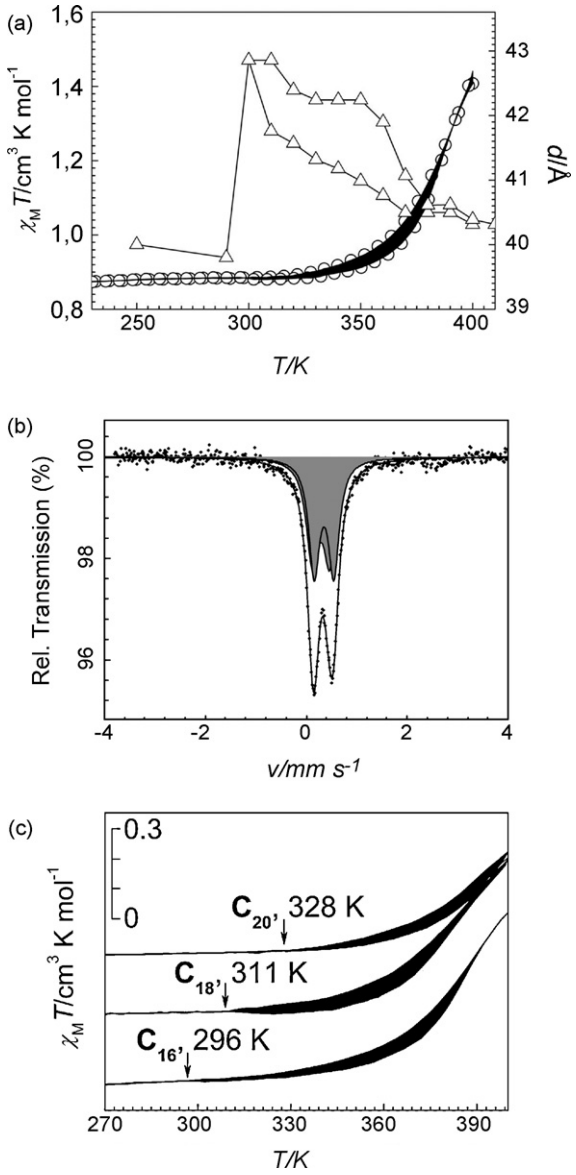

Fig. 3. (a) $\chi_M T$ vs. T for **C_{16}-1**$\cdot0.5H_2O$ and variation of the distance d with temperature (△) deduced from XPRD profiles after following the sequence 310–410–230–410 K. (b) Mössbauer spectrum of **C_{16}-1**$\cdot0.5H_2O$ measured at 80 K (LS doublet: dark grey). (c) $\chi_M T$ vs. T for **C_n-1**$\cdot0.5H_2O$ (n = 16, 18 and 20), arrows indicate the temperatures at which the heating and cooling curves diverge. The black areas indicate the hysteresis loops.

Table 1
Interlayer distances *d* at different temperatures, thermal transitions and mesomorphism determined by XPRD, DSC, TGA and POM for compounds **C_n-1**–**C_n-7**.

Code	Compound	*d* [Å]		Thermal transitions [K][b]
		300 K	410 K	
C_{16}-1·3.5H_2O	[Fe(C_{16}-trenH)]Cl_2 3.5H_2O	34.7		$Cr \overset{335}{\rightleftharpoons} S_A$
C_{16}-1·0.5H_2O	[Fe(C_{16}-trenH)]Cl_2 0.5H_2O	38.7	39.1	$Cr \overset{287}{\underset{270}{\rightleftharpoons}} S_A$ 456 i(d)
C_{18}-1·3.5H_2O	[Fe(C_{18}-trenH)]Cl_2 3.5H_2O	36.0		$Cr \overset{325}{\rightleftharpoons} S_A$
C_{18}-1·0.5H_2O	[Fe(C_{18}-trenH)]Cl_2 0.5H_2O	40.1	42.3	$Cr \overset{301}{\underset{287}{\rightleftharpoons}} S_A$ 463 i(d)
C_{20}-1·3.5H_2O	[Fe(C_{20}-trenH)]Cl_2 3.5H_2O	37.7		$Cr \overset{352}{\rightleftharpoons} S_A$
C_{20}-1·0.5H_2O	[Fe(C_{20}-trenH)]Cl_2 0.5H_2O	44.1	45.0	$Cr \overset{330}{\underset{320}{\rightleftharpoons}} S_A$ 449 i
C_6-2	[Fe(C_6-trenH)]$(ClO_4)_2$	16.592(5)[a]	–	–
C_{18}-2	[Fe(C_{18}-trenH)]$(ClO_4)_2$	29.1	31.05	$Cr \overset{380}{\underset{355}{\rightleftharpoons}} S_X$ 473 d
C_{12}-3	[Fe(C_{12}-tameMe)]$(BF_4)_2$	26.6	29.4	$Cr \overset{361}{\underset{349}{\rightleftharpoons}} S_X$ 500 d
C_{14}-3	[Fe(C_{14}-tameMe)]$(BF_4)_2$	27.1	30.3	$Cr \overset{369}{\underset{360}{\rightleftharpoons}} S_X$ 490 d
C_{16}-3	[Fe(C_{16}-tameMe)]$(BF_4)_2$	28.1	32.1	$Cr \overset{377}{\underset{365}{\rightleftharpoons}} S_X$ 510 d
C_6-4	[Fe(C_6-tameMe)]$(ClO_4)_2$	18.087(7)[a]	–	–
C_{18}-4	[Fe(C_{18}-tameMe)]$(ClO_4)_2$	33.3	35.7	$Cr \overset{397}{\underset{383}{\rightleftharpoons}} S_X$ 506 d
C_8-5	[Fe(C_8-tba)$_3$]$(4\text{-}MeC_6H_4SO_3)_2$	25.9	–[c]	g $\overset{277}{\searrow}$ Col_h (LS $\overset{340}{\searrow}$ HS) $\overset{462}{\searrow}$ i $\overset{511}{\searrow}$ d
C_{10}-5	[Fe(C_{10}-tba)$_3$]$(4\text{-}MeC_6H_4SO_3)_2$	27.1	–[c]	g $\overset{295}{\searrow}$ Col_h (LS $\overset{343}{\searrow}$ HS) $\overset{460}{\searrow}$ i $\overset{500}{\searrow}$ d
C_{12}-5	[Fe(C_{12}-tba)$_3$]$(4\text{-}MeC_6H_4SO_3)_2$	29.0	–[c]	g $\overset{265}{\searrow}$ Col_h (LS $\overset{341}{\searrow}$ HS) $\overset{463}{\searrow}$ i $\overset{510}{\searrow}$ d
C_{10}-6	[Fe(C_{10}-tba)$_3$]$(CF_3SO_3)_2$	29.1	–[c]	g $\overset{271}{\searrow}$ Col_h (LS $\overset{299}{\underset{294}{\rightleftharpoons}}$ HS) $\overset{514}{\searrow}$ d
C_{12}-6	[Fe(C_{12}-tba)$_3$]$(CF_3SO_3)_2$	29.8	–[c]	g $\overset{273}{\searrow}$ Col_h (LS $\overset{297}{\underset{293}{\rightleftharpoons}}$ HS) $\overset{507}{\searrow}$ d
C_6-7	[Fe(C_6-trenMe)]$(ClO_4)_2$	17.461(6) (90 K) 17.870(9) (298 K)[a]	–	–
C_{12}-7	[Fe(C_{12}-trenMe)]$(ClO_4)_2$	24.0	24.8	$Cr \overset{370}{\underset{367}{\rightleftharpoons}} S_X$ 500 d
C_{18}-7	[Fe(C_{18}-trenMe)]$(ClO_4)_2$	29.6	31.3	$Cr \overset{382}{\underset{367}{\rightleftharpoons}} S_X$ 470 d

[a] From the monocrystal X-ray data.
[b] Measured by DSC on the second heating–cooling cycle. The identification of the mesophase was done on the basis of POM and XPRD data.
[c] No variation of the interlayer distance *d* is observed.

smectic mesophase S_A has been identified with layered structures similar to **C_6-2** (Fig. 2b). Table 1 gathers the critical temperatures of melting, isotropization and decomposition deduced from DSC, POM and thermogravimetric analysis.

Fig. 3c displays the $\chi_M T$ vs. *T* plots for **C_n-1**·0.5H_2O (*n* = 16, 18 and 20), where χ_M stands for the magnetic susceptibility and *T* the temperature. The Mössbauer spectrum recorded for the derivative with *n* = 16 at 80 K is also shown (Fig. 3b). The compounds adopt the LS state in the temperature interval of 4.2–290 K where the Mössbauer spectra indicate the presence of small residual HS fraction. For all these derivatives the $\chi_M T$ vs. *T* between 400 and 296 K presents a variation accompanied by a narrow hysteresis (Fig. 3c). Below 296 K $\chi_M T$ remains almost constant until 10 K where it sharply decreases as a consequence of the zero field splitting of the Fe(II) ions remaining in the HS state [18]. The thermally induced spin transition in **C_n-1**·0.5H_2O starts right after the onset of the first order phase transition ($Cr \leftrightarrow S_A$). Since the spin transition is blocked below the temperature at which the compounds solidify one can conclude that the melting process drives the spin transition in these metallomesogens. The fact that the spin transition inside the S_A mesophase is accompanied by hysteresis is due to the structural reorganization of the metallomesogen upon $Cr \leftrightarrow S_A$ transition. It is worth mentioning that the spin transition temperature is determined by the melting temperature which is higher for the derivatives with longer alkyl chains (Fig. 3c, Table 1). These compounds are dark purple in the LS state and become light purple-brown in the HS state [18].

2.2. Type ib: structural changes associated with the Cr ↔ LC influence the spin state of the metallic centers but they are not the driving force of the spin transition

Complexation of the ligand C_n-tameMe (2,2,2-tris(2-aza-3-((5-akloxy)(6-methyl)(2-pyridyl))prop-2-enyl)ethane) with $Fe(BF_4)_2 \cdot 6H_2O$ salts have afforded a family of complexes with general formula [Fe(C_n-tameMe)]$(BF_4)_2$ (**C_n-3**) with *n* = 12, 14, 16 [19] (Fig. 1b). Single crystal X-ray measurements have been performed on the analogue [Fe(C_6-tameMe)]$(ClO_4)_2$ (**C_6-4**) at 100 K. The complex crystallizes in the triclinic system and adopts the *P*bca space group. The iron(II) ion is in a distorted octahedral environment shaped by three imine and three pyridine nitrogen atoms of the C_n-tameMe ligand (Fig. 4a). The average $Fe–N^{im}$ and $Fe–N^{py}$ bond distance is 1.918(2) and 2.084(2) Å, respectively, which are characteristic for the Fe(II) ion in the LS state. The distance between methyl groups and adjacent nitrogen atoms of pyridine rings is 3.040(3) Å. Neighbouring molecules are packed in a head-to-head fashion forming a layered microsegregated structure (Fig. 4b). The ionic layer is composed of cationic SCO head groups and perchlorate anions, whereas alkyl tails are arranged into a non-polar hydrocarbon layer. Within the ionic layers short CH···O(Cl) contacts are present (2.444(2)–2.711(2) Å). Each alkyl chain introduces a single *gauche* kink in the bonds next to the oxygen atom to allow for the tilt alignment, whereas the remaining carbon bonds remain in the *trans* configuration. Poorly aligned short alkyl chains of adjacent layers interpenetrate defining a

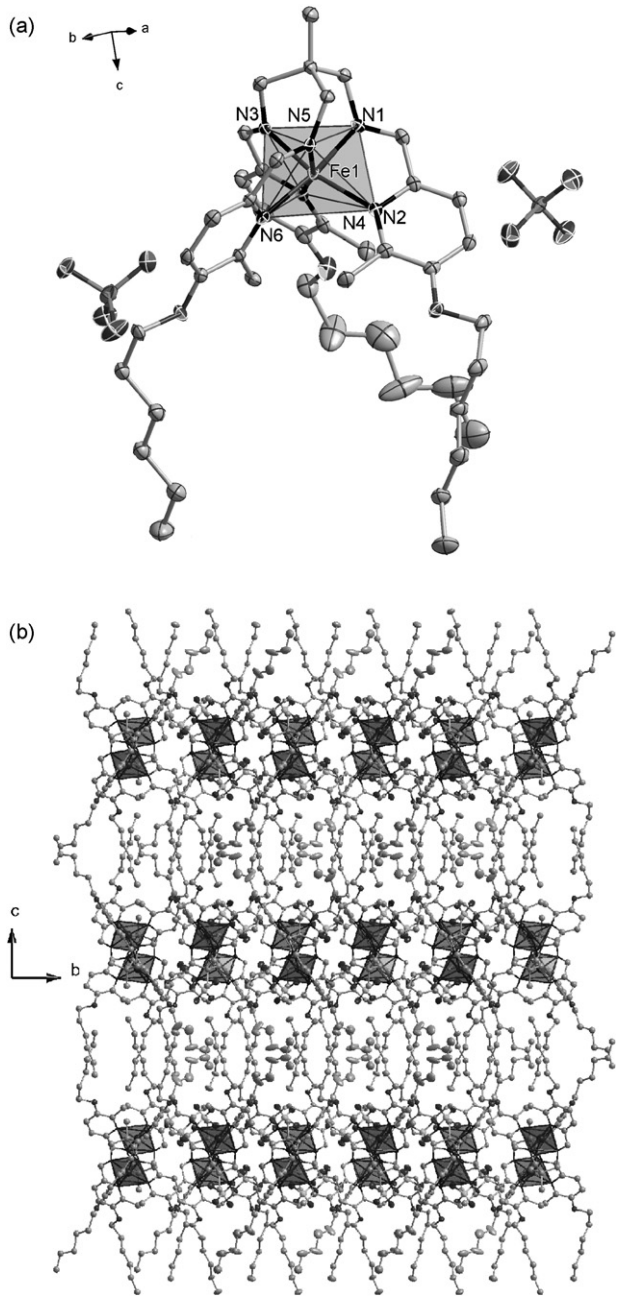

Fig. 4. (a) Projection of the cation $[Fe(C_6\text{-tameMe})]^{2+}$ in **C_6-4** at 100 K; hydrogen atoms are omitted for clarity. Displacement ellipsoids are shown at 50% probability level. (b) Projection of the molecular packing of **C_6-4** along the *a* axis. Hydrogen atoms and perchlorate anions are omitted for clarity.

kind of paraffin sublattice with distorted hexagonal ordering. The distance between neighbouring layers is 18.087(7) Å.

The variable temperature XRPD patterns have been recorded following the sequence 310–410–310–410 K for compounds **C_n-3** with $n = 12$, 14, 16. The compounds exhibit a lamellar structure, indicated by the powder XRPD patterns displaying intense low angle reflections together with the second and higher reflections, all corresponding to the stacking periodicity of the layers [19]. The other observed reflections are much smaller in intensity, which is characteristic of long alkyl-chain materials because of the extremely high degree of preferred orientation [24]. Upon heating the change of the high-angle alkyl peak with concomitant increase of the interlayer distance is seen in the variable temperature XRPD profiles [19]. This behaviour can be assigned to the melting of alkyl chains. In accordance with the detected increase of the layer thickness with melting and absence of further variation of it with temperature the observed mesophases might be assigned to the smectic type [25].

The interlayer distance *d* at different temperatures calculated from the Bragg's equation is shown together with the magnetic data in Fig. 5a–c. As is seen, the anomalous change of the magnetic susceptibility is synchronous with the abrupt change of the interlayer distance *d* (Fig. 5a–c, right scale). The *d* vs. *T* plot presents a hysteresis loop due to supercooling during transition from the mesophase to the crystal state for all compounds. This observation indicates that the mesophase possesses some degree of crystalline order [26]. The structural transition from the low-temperature phase (Cr) to the high-temperature phase (S_X) coincides with the observed magnetic hysteresis loop.

The three homologues in the series with $n = 12$, 14, 16 are in the LS state at 275 K (Fig. 5a–c) as indicated by the $\chi_M T$ values. The Mössbauer spectra measured at 80 K (shown as inserts in Fig. 5a–c) confirm that practically all Fe(II) ions are in the LS state. As the temperature increases, $\chi_M T$ continuously adopts higher values as a consequence of the thermal spin transition of more than 75% of the Fe(II) ions (inferred from the $\chi_M T$ value at 350 K). Above 350 K, the $\chi_M T$ values show a discontinuity in the heating and cooling curves, which do not coincide in the temperature range but in shape of the hysteresis loop. The center of the magnetic discontinuity is located at 356, 368 and 375 K, for derivatives with $n = 12$, 14 and 16, respectively. The hysteresis loop of the homologue with $n = 16$ has a width of 10 K and is rate dependent. Increasing the heating/cooling rates from 0.1 up to 10 K min^{-1} almost doubles the width of the loop [19]. Successive thermal cycles did not modify the shape of it. It was also checked that the loop does not depend on the magnitude of the field applied up to 7 T [19]. The decrease of the magnetic susceptibility upon heating as observed for these complexes is in contrast to the normally observed behaviour of spin crossover compounds [12,27] suggesting to be a direct influence of the Cr ↔ S_X phase transition. In fact, the *d* vs. *T* plots demonstrate that the discontinuity in *d* takes place in the same temperature interval where the magnetic change occurs.

At 293 K, the distance *d* for pristine compounds displays the values of 26.6 Å ($n = 12$), 27.1 Å ($n = 14$) and 28.5 Å ($n = 16$) (Table 1). They remain constant up to approximately 350 K where they abruptly increase adopting values of 29.4 Å ($n = 12$), 30.3 Å ($n = 14$) and 32.1 Å ($n = 16$) at 400 K as a consequence of the melting process. The structural intramolecular and intermolecular reorganization of the $[Fe(C_n\text{-tameMe})]^{2+}$ cations on going to the mesophase is notably reflected in their magnetic properties. It provokes a decrease in the $\chi_M T$ value of *ca.* 0.5 cm^3 K mol^{-1} between 350 and 370 K. It can be inferred from these $\chi_M T$ values that 14% of the HS $[Fe(C_n\text{-tameMe})]^{2+}$ cations have changed to the LS state. In the first cooling solidification takes place around 356 K ($n = 12$), 369 K ($n = 14$) and 377 K ($n = 16$) and the *d* vs. *T* plot presents a 6–10 K hysteresis width due to the supercooling of the mesophase (Fig. 5a–c). The hysteresis cycle is also noticeable in the $\chi_M T$ vs. *T* plot in the same temperature interval. After solidification the compounds adopt the original spin state with the fraction of molecules in the HS state restored. The reversibility and reproducibility of the Cr ↔ S_X transition has been proved after several cycles of heating and cooling. A small fraction of molecules of *ca.* 14% undergo spin state change as a consequence of the structural reorganization of the metallomesogen upon Cr ↔ S_X transition. It notably affects the thermally driven SCO process in **C_n-3** with $n = 12$, 14, 16. The cooperativity of the SCO process seems not to be strongly influenced by the change of aggregate of matter. The spin crossover process is continuous both in the crystal and liquid state although less cooperative in the liquid state. The simulation of the spin transition curve for these compounds before and after melting was

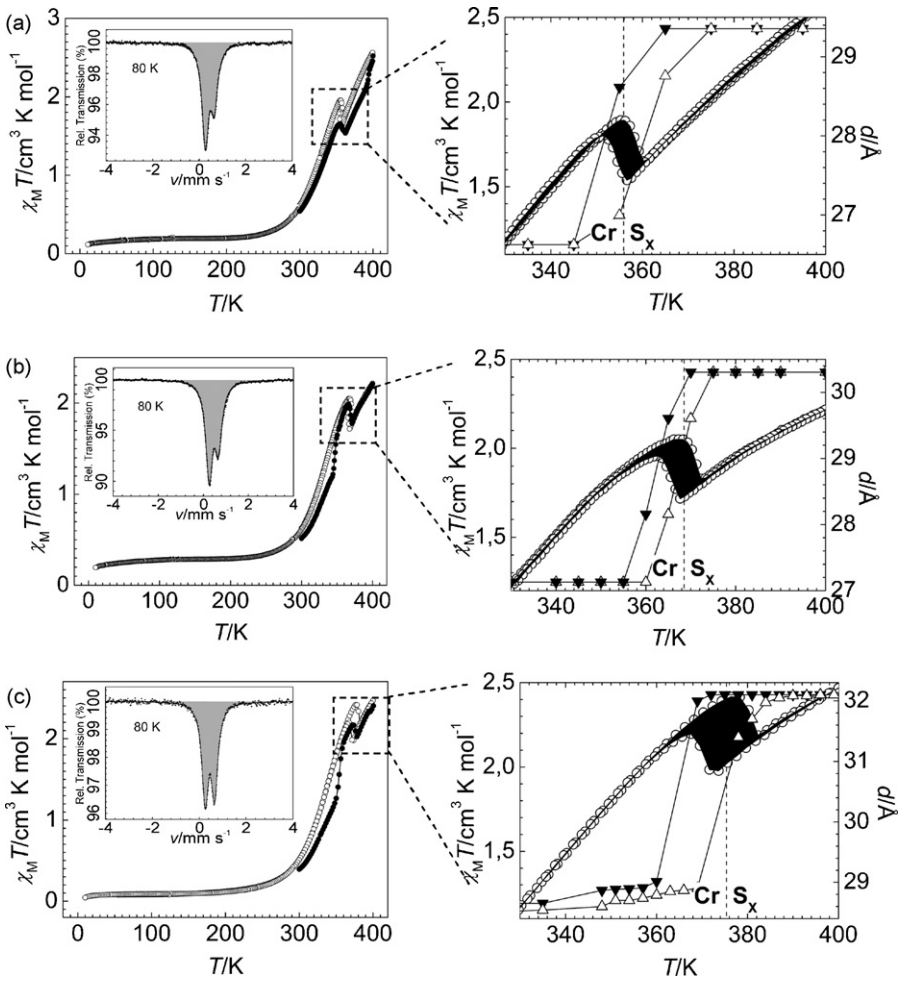

Fig. 5. Left: Magnetic susceptibility curves for **C*n*-3** $n = 12$ (a), 14 (b), 16 (c) in the form $\chi_M T$ vs. T (symbol ○, first heating–cooling run; symbol ●, subsequent cycles) and Mössbauer spectra measured at 80 K. Right: Temperature dependence of the interlayer distance d. Symbol ▼ corresponds to the interlayer distance d measured during the first cooling and the second heating runs (symbol △).

performed using the equation derived from the regular solution model [28]. The least squares fitting leads to similar thermodynamical parameters $\Delta H = 22.3$ and 21.9 kJ mol^{-1}, and $\Delta S = 63.5$ and 59.3 J K^{-1} mol^{-1} before and after melting, respectively. This corresponds to $T_{1/2}{}^{solid} = 351$ K and $T_{1/2}{}^{mesophase} = 369$ K. The interaction parameters Γ is 2.2 kJ mol^{-1} in solid state and 1.9 kJ mol^{-1} in the mesophase. According to the structural and DSC analysis, on melting a modification of intermolecular contacts takes place, which is responsible for the change of the thermodynamical parameters $T_{1/2}$ and Γ in two phases (Fig. 6, top). As is seen, in the solid-state interactions between molecules are more cooperative and become less cooperative after melting of the alkyl chains (Fig. 6, bottom). However, the transition is still rather cooperative that means retaining in part the crystal ordering within the ionic bilayers. According to the classification given by comparison with $2RT_{1/2}$, the spin transition in both phases can be considered as being moderately cooperative [27,28].

Summarizing, these zero-dimensional Fe(II) spin crossover metallomesogens exhibit coupled spin state and Cr ↔ S_X phase transitions around room temperature. However, at variance with precedent systems of type (a) [18], these metallomesogens undergo thermally driven spin transition and the solidification ↔ melting process only affects the spin transition process by modifying slightly its completeness and cooperativity. Compounds **C*n*-3** show thermochromic properties, they are dark violet in the LS state ($T < 275$ K, Cr) and become red in the HS state ($T > 275$ K, Cr, S_X).

2.3. Type ic: g ↔ LC pseudo-second order phase transition influence the thermally driven spin transition of the metallic centers

Interplay between spin state transition and g ↔ Col_h pseudo-second order phase transition has been observed in the one-dimensional Fe(II) metallomesogens with formula $[Fe(C_n\text{-tba})_3](X)_2$ [C_n-tba = 3,5-bis(alkoxy)-*N*-(4*H*-1,2,4-triazol-4-yl)benzamide, X = 4-Me$C_6H_4SO_3^-$ (**C*n*-5**), $CF_3SO_3^-$ (**C*n*-6**) and $n = 8$, 10, 12] [20,21].

The polymeric structure of these compounds has been proven by an EXAFS study, which shows a similar linear local structure (changing the triazole ligand and the counterions) as that observed in the precedent triazole coordination compounds (Fig. 7) [29,30].

The XPRD profiles of the complexes **C*n*-5** with $n = 8$, 10, 12 have been measured in the 170–375 K temperature range [21]. A discotic columnar mesophase Col_h has been identified for all homologues, which has also been confirmed by POM. Realization of the crystalline state in these compounds is difficult; only for the homologue with longer alkyl chains was observed an endothermic peak in the DSC profiles at 270 K with high energy, which originates from the transition glass → columnar hexagonal. The XPRD data did not unravel any structural change on going from 230 K up to 300 K. Since this broad peak in the DSC profiles is observed in the first heating run of all these derivatives which are completely low spin, we accepted the possibility of the glass transition (vitrification). In

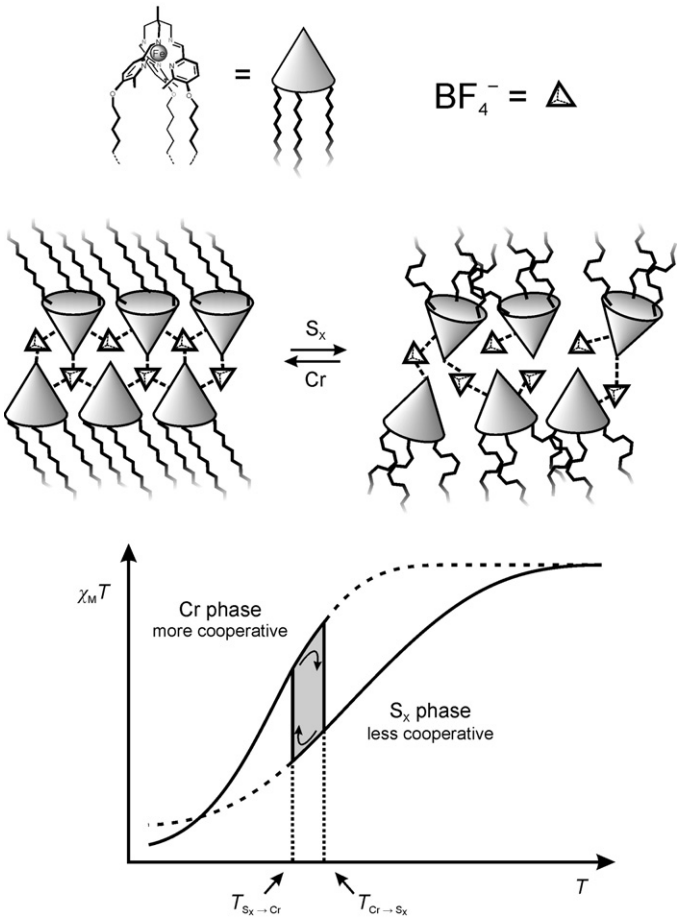

Fig. 6. Proposed organization of the ionic bilayers of **C_6-3** in crystalline state (Cr) and smectic mesophase (S_X) with intermolecular contacts represented by dashed lines. On the bottom are schematized the plots of the transition corresponding to the crystalline and smectic phases near the temperature of the phase transition. Dashed lines show the hypothetical shape of the curves in absence of the phase transition.

Table 1 are gathered the thermal transitions deduced from DSC, POM and TGA experiments.

The magnetic investigation revealed for these compounds an incomplete spin transition accompanied by hysteresis and colour change in the temperature region of 250–300 K (Fig. 8a–c). Around 50% of iron(II) ions change the electronic configuration as can be inferred from the value of $\chi_M T$ at 200 K. In fact, the Mössbauer spectrum recorded for the compound with $n = 10$ at 4.2 K demonstrates that 50% of the iron(II) ions are in the low spin state (Fig. 8b). Further decrease of the $\chi_M T$ value below 100 K is due to zero-field splitting and possibly antiferromagnetic coupling of the iron(II) atoms remaining in the high spin state [29]. The temperature and abruptness of the spin transition and the hysteresis width increase upon increasing n, despite non-linearly. The hysteresis of the magnetic properties is a feature resulting from the operation of the liquid crystallinity alone. Another remarkable fact is that the spin transition in these compounds became frozen below *ca.* 250 K. A residual high spin fraction of *ca.* 50% is unusual and is due to the vitrification of the compounds, which provokes an inhibition of the spin transition process. The temperature of vitrification in these compounds changes non-linearly with the alkyl chain length with the highest temperature being observed for the homologue with $n = 10$.

The compounds **C_n-6** with $n = 10$, 12 present similar mesomorphic behaviour as that observed for $MeC_6H_4SO_3^-$ derivatives; however, they undergo complete thermal spin transition above 300 K accompanied by small hysteresis loops (Fig. 9a and b) [20]. The magnetic hysteresis loop can by no means be attributed to the increase of the interchain cooperativity. The explanation should be looked for in the fact that those compounds down to 295 K ($n = 10$) and 275 K ($n = 12$) are in the liquid crystalline state as was determined by XRPD, DSC and POM measurements (Table 1). The width of the loop is quite small (~2 K) which points out that upon spin transition the liquid crystalline compounds exhibit relatively small structural reorganization. Additionally, the complicate form of the loop for the derivative with $n = 12$ points at a direct influence of the glass transition on the magnetic properties. The feature detected at the low temperature edge near 275 K coincides with the anomaly detected by the XRPD and DSC techniques.

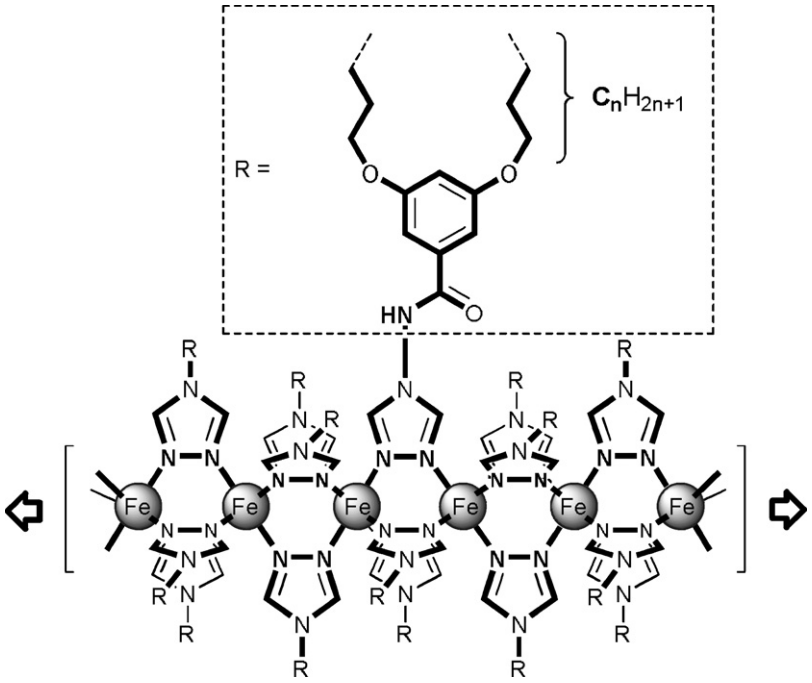

Fig. 7. Illustration of the polymeric structure of compounds **C_n-5** and **C_n-6** ($n = 8$, 10, 12).

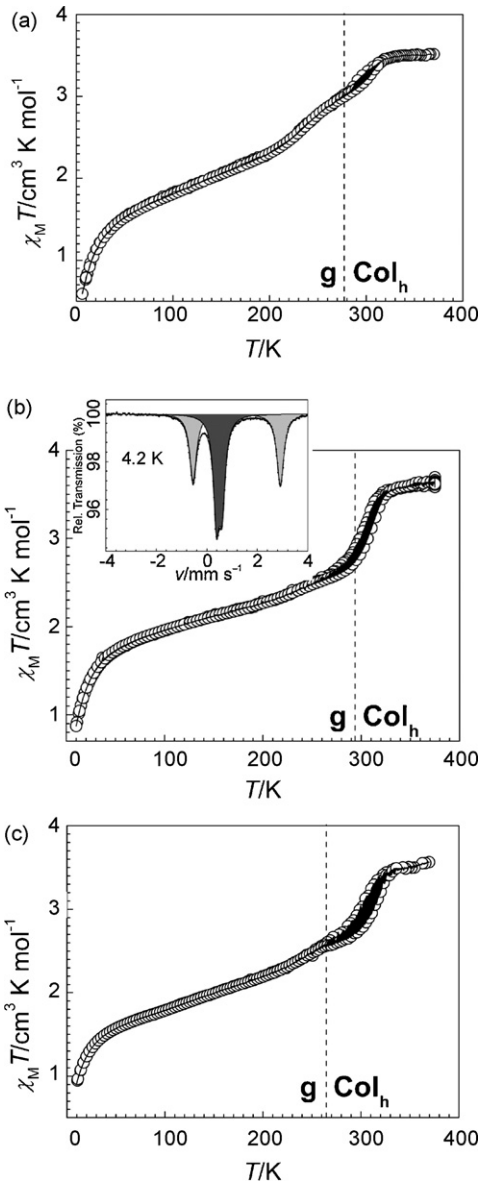

Fig. 8. Magnetic susceptibility curves for $\mathbf{C_n}$**-5** with $n = 8$ (a), 10 (b) and 12 (c) in the form $\chi_M T$ vs. T. The black areas indicate the hysteresis loops. The dashed lines indicate the temperature of the vitrification (T_g). The Mössbauer spectrum measured at 4.2 K is shown for the derivative with $n = 10$ (HS: light grey doublet, LS: dark grey doublet).

As discussed in literature [31] the interchain interactions in triazole-based spin crossover polymers are important for the appearance of the abruptness and hysteresis of the spin transition. But as we have shown [20] in the alkylated system upon passing some threshold of the chain length a new effect comes into play which modifies the characteristics of the spin transition. This effect is liquid crystallinity. The semi-fluid nature of the liquid crystalline materials is responsible for the delay effect in the restoring of the magnetic properties upon subsequent heating/cooling.

An interesting and important feature is the possibility to obtain these materials in the form of thin films. In a separate experiment, *ca.* 10 mg of complexes were dissolved in $CHCl_3$ (1 mL) and subsequently the solution layered onto a glass plate and allowed the solvent to evaporate. Thin films of a few μm thick form after solvent evaporation. Reversible change between violet (LS state) and white (HS state) colouration of the films by heating or cooling around 300 K was observed without fatigue (Fig. 10).

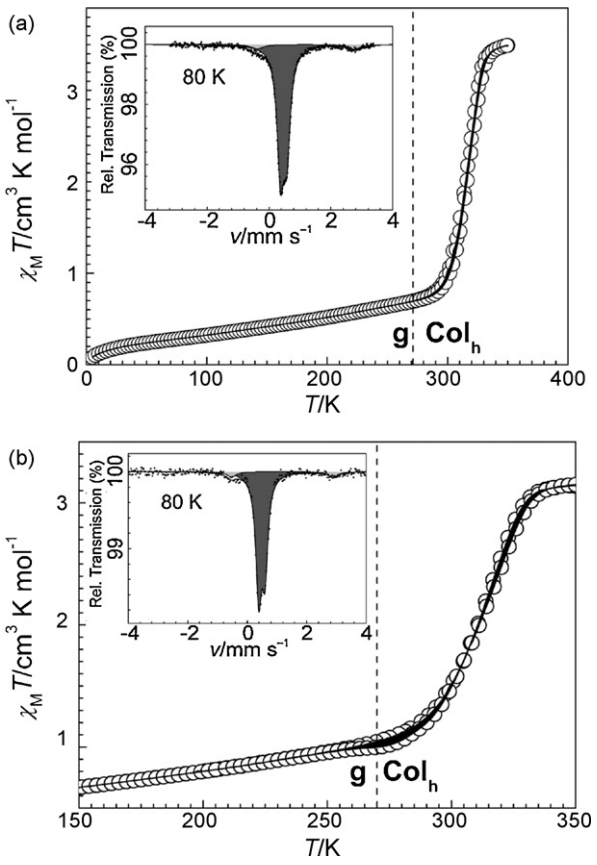

Fig. 9. Magnetic susceptibility curves for $\mathbf{C_n}$**-6** with $n = 10$ (a) and 12 (b) in the form $\chi_M T$ vs. T. The black areas indicate the hysteresis loops. The dashed lines indicate the temperature of the vitrification (T_g). The Mössbauer spectra were measured at 80 K (HS: light grey doublet, LS: dark grey doublet).

3. Fe(II) metallomesogens with coexisting but uncoupled spin state and liquid crystal phase transition due to competition with the dehydration in the same temperature interval (type ii)

The compounds $\mathbf{C_n}$**-1**·3.5H_2O, $n = 16$, 18, 20 show a very particular spin state change [18]. Fig. 11a illustrates the $\chi_M T$ vs. T plot for the compound $\mathbf{C_{16}}$**-1**·3.5H_2O together with the corresponding Mössbauer spectrum recorded at 80 K. This compound is in the LS state at 300 K as confirmed by the $\chi_M T$ value of 0.02 cm^3 K mol^{-1} as well as by the Mössbauer spectrum. Upon heating $\chi_M T$ increases abruptly, attaining the value of 1.75 cm^3 K mol^{-1} at 400 K, where around 50% of the Fe(II) ions have converted to the HS state. The TGA have shown that dehydration takes place in the same temperature region where the spin state change occurs. Additionally, DSC

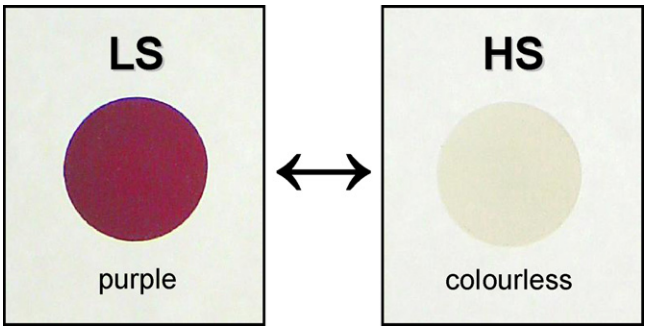

Fig. 10. Change of colouration in the films of compounds $\mathbf{C_n}$**-5** and $\mathbf{C_n}$**-6** ($n = 8$, 10, 12) upon spin transition.

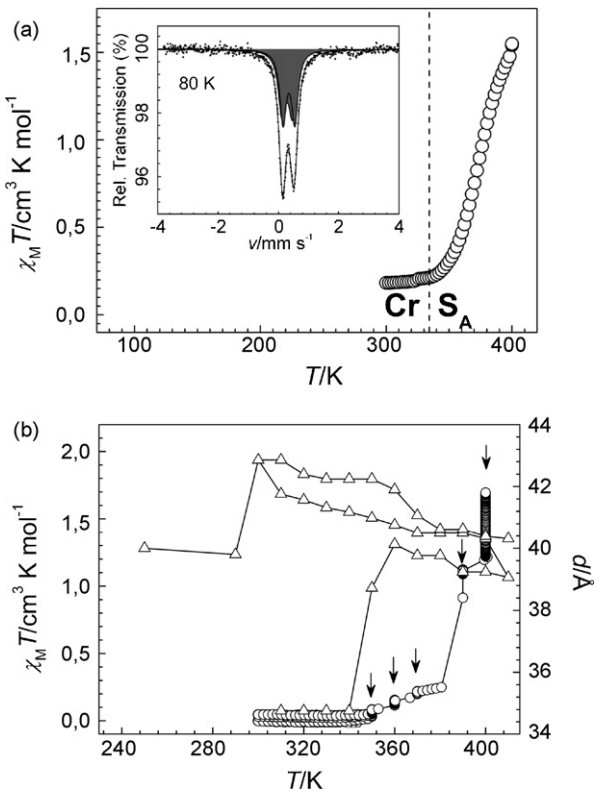

Fig. 11. (a) Magnetic susceptibility curve for **C_{16}-1**·3.5H_2O in the form $\chi_M T$ vs. T together with the Mössbauer spectrum measured at 80 K (LS: dark grey doublet). The dashed line indicates the temperature of Cr ↔ S_A. (b) Variation of the distance d with temperature (△) in **C_{16}-1**·3.5H_2O deduced from XPRD profiles after following the sequence 310–410–230–410 K together with dehydration experiments monitored by the temperature dependence of the magnetic susceptibility. The hydrated samples were placed in open containers in the SQUID sample holder and their magnetism measured. The first part of the experiment comprised several cycles of heating–cooling from 280 until 350 K (empty squares). Then, the samples were left for 2 h at the reported temperatures (indicated by arrows) and the magnetic moment was measured (open circles). Dehydration taking place under these conditions is confirmed by the thermogravimetric analysis.

profiles, POM analysis and XPRD patterns show that the melting occurs at 340 K (first heating scan) (Table 1). At this point the following question has emerged: does the solid ↔ liquid crystal phase transition during the first heating drive the spin transition in **C_{16}-1**·3.5H_2O or is it caused by the loss of water?

In order to answer this question we have performed dehydration experiments monitoring the temperature dependence of the magnetic susceptibility (Fig. 11b) and have recorded temperature dependent XPRD patterns following the sequence 310–410–230–410 K. The sample was heated and subsequently cooled during several cycles between 280 K (LS state) and 350 K. The $\chi_M T$ value after three cycles of melting ↔ solidification (287 K second heating scan) does not show any noticeable variation. In addition, the temperature variation of d derived from XPRD patterns (Fig. 11b) presents an abrupt increase as a consequence of the melting between 340 and 350 K, but the increase in the $\chi_M T$ value begins at 360 K. Consequently, the hypothesis that the phase transition to the mesophase drives the spin state change can be ruled out, at least in the present compound. On the contrary, it is clearly seen in the dehydration experiments that the magnetic susceptibility increases upon losing water, which matches with reported TGA data, and is completely accomplished at 400 K. For this compound 50% of the Fe(II) ions undergo spin state change at $T_{1/2}$ = 375 K induced by releasing water. Synergy between desolvation and spin state change as observed in this compound has been reported in several cases [27]. One remarkable fact is that the analogues with longer alkyl chains as well as the compound [Fe(C_{18}-tren)]F_2·3.5H_2O behave similarly as **C_{16}-1**·3.5H_2O [18].

Other examples of spin state change due to dehydration have been found in one-dimensional Fe(II) metallomesogens [21]. The compounds **C_n-5**·H_2O (n = 8, 10 and 12) are in the LS state at 293 K where they present the Col_h mesophase. Upon heating $\chi_M T$ increases abruptly within a few Kelvin clearly indicating the change of spin state, which additionally is accompanied by a pronounced change of colour [from purple (LS state) to white (HS state)]. TGA and magnetic measurements have shown that the spin state change takes place concomitantly with the dehydration of the compounds.

4. Fe(II) metallomesogens with uncoupled spin state and liquid crystal phase transition (type iii)

The compound **C_{18}-2** adopts the LS state in the temperature region between 10 and 400 K, where the temperature dependence of the magnetic susceptibility has a constant value of 0.10 cm^3 $K mol^{-1}$. The Mössbauer spectrum recorded at 80 K indicates only one LS doublet (Fig. 12) [18].

Introduction of the methyl group in the C_n-trenR ligand has resulted in a noticeable modification of the crystal field strength at the iron(II) center. The coordination of the ligand C_n-trenMe (tris[3-aza-4-((5-C_n)(6-methyl)(2-pyridyl))but-3-enyl]amine) has afforded a series of compounds with general formula [Fe(C_n-trenMe)]$(ClO_4)_2$ (**C_n-7**) with n = 6, 12 and 18 [18] (Fig. 1c). For [Fe(C_6-trenMe)]$(ClO_4)_2$ (Fig. 13a) the average Fe(II)–N bonds (2.007(1) Å) and the distortion parameter Σ (85.54(7)°) at 90 K are characteristic of the LS state while at 298 K they are typical for the HS state (2.234(3) Å, 116.59(11)°). Modifications of the coordination sphere of **C_6-7** due to spin transition are directly reflected on the metal-to-ligand bond length, which is illustrated by the distinguishable divergence of the overlapped HS and LS structures (Fig. 13b). In the HS form the distances Fe-N(ligand) are longer, consequently, the volume of the [FeN_6] chromophore increases. The compound **C_6-7** displays similar crystal packing like that observed in **C_6-2** [18] despite both compounds crystallize in different space groups. The crystal packing in the LS and HS structures for **C_6-7** is almost identical, with CH···O(Cl) contacts being 2.308(5)–2.781(5) Å (HS) and 2.301(5)–2.718(5) Å (LS).

The compounds **C_n-7** n = 6, 12 and 18 exhibit spin crossover behaviour at $T_{1/2}$ centered around 140 K, the temperature at which the number of molecules in the HS and LS states is equal (Fig. 14a). The spin transition is complete and relatively continuous with $T_{1/2}$ = 146, 120 and 133 K, for analogues with n = 6, 12 and 18,

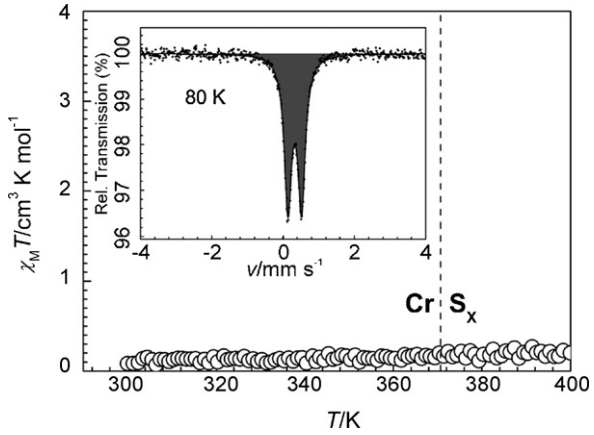

Fig. 12. Magnetic susceptibility curve for **C_{18}-2** in the form $\chi_M T$ vs. T together with the Mössbauer spectrum measured at 80 K (LS: dark grey doublet). The dashed line indicates the temperature of Cr ↔ S_X.

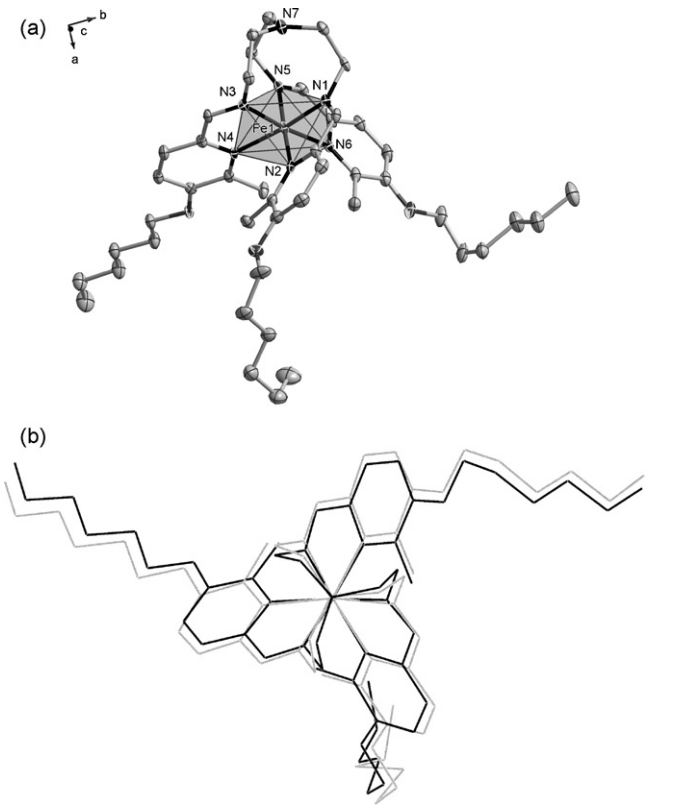

Fig. 13. (a) Projection of the cations $[Fe(C_6\text{-trenMe})]^{2+}$ in **C_6-7** at 90 K. Displacement ellipsoids are shown at 50% probability level. (b) Projection along Fe···N7 axis of the minimized overlay of the cation $[Fe(C_6\text{-trenMe})]^{2+}$ in the LS state at 90 K (dark grey) and in the HS state at 298 K (light grey).

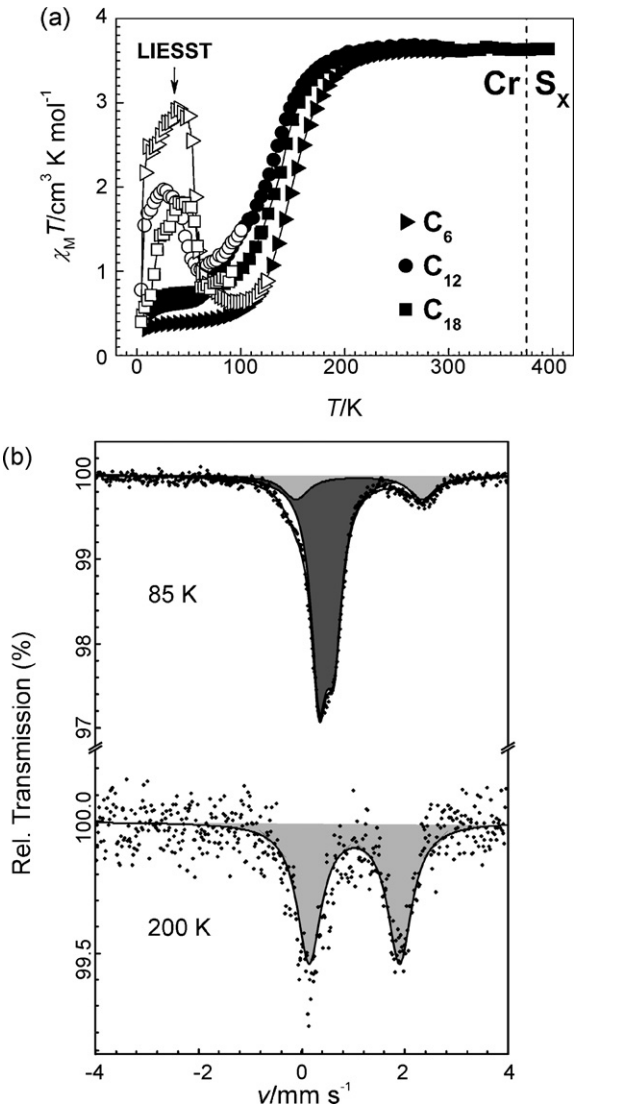

Fig. 14. (a) Magnetic properties in the form of $\chi_M T$ vs. T for **C_n-7** with $n = 6$, 12 and 18 and LIESST experiments with irradiation and subsequently moving up in temperature (open symbols). The sample was irradiated at 4 K (LS state) with light of $\lambda = 514$ nm (25 mW cm^{-2}) until saturation of the magnetic moment was reached. Then irradiation was switched off and $\chi_M T$ vs. T was recorded in the warming mode at a rate of 2 K min^{-1} up to 300 K. At temperatures higher than 70 K, $\chi_M T$ increases following the spin transition curve observed for each compound. The dashed line corresponds to the transition Cr ↔ S_X of **C_{18}-7**; (b) Mössbauer spectra of derivative with $n = 18$ measured below and above the transition temperature.

respectively. Mössbauer spectra recorded below and above $T_{1/2}$ for all analogues are consistent with the reported magnetic and structural data (Fig. 14b). The thermal spin transition is accompanied by a pronounced change of colour from dark red (LS) to orange (HS). The LIESST effect [14] has been investigated in these compounds. The LS ground state was photo-converted at 4 K to a metastable HS state after irradiation of the samples with light of $\lambda = 514$ nm (25 mW cm^{-2}) (Fig. 14a). The highest percentage of molecules that was photo-converted to the HS state inferred from $\chi_M T$ values at 42, 25 and 42 K for analogues with $n = 6$, 12 and 18 is 80%, 54%, 50%, respectively. The critical temperature of relaxation of the metastable HS state known as T^{LIESST} [14] is 56 K ($n = 6$), 48 K ($n = 12$) and 56 K ($n = 18$).

XPRD profiles of the complexes **C_{18}-2** and **C_n-7** ($n = 12$ and 18) have been recorded at 300 and 410 K. The X-ray diffraction patterns of the mesophase of these complexes gave a single sharp low angle (10) reflection and weak high-order reflection(s) all corresponding to the layer spacing. An additional diffuse reflection observed at larger angles refers to the average lateral spacing between alkyl chains. On the basis of these observations at high temperature a smectic mesophase S_X has been identified for all derivatives with layered structures similar to **C_6-2** and **C_6-7**. Table 1 gathers the critical temperatures of melting, isotropization and decomposition deduced from DSC, POM and TGA measurements.

The lengthening of alkyl chains in **C_n-7** provokes a decrease of $T_{1/2}$, however, not in a linear way. In fact, these compounds are obtained in the HS form at ambient temperature, and they adopt packing of molecular parts favoring bulkier HS polar heads. This could play a role in the shift of SCO in higher homologues to lower temperatures compared to the one observed in **C_6-7**. Packing long alkyl chains to some extent may prevent contraction of the cavity within the trifurcated ligand with an encapsulated iron(II) ion. The effect is rather weak causing the shift to lower temperature by ~15 K for the analogue with $n = 18$.

5. Discussion

According to Sorai, phase transitions taking place in condensed matter manifest themselves as concerted effects of molecular structure, intermolecular interactions, and molecular motions [32]. Well-known phase transitions include the order–disorder, displacive and reconstructive types. The order–disorder type phase transition involves a change in the positional and orientational alignment of molecular or spin axes [33]. The displacive-type phase transition concerns the displacement of atomic or molecular positions preserving the existing bonds [33]. The reconstructive transition is the most drastic and involves considerable atomic movements [33]. Since intramolecular electronic energy is much greater than intermolecular potential energy, the change in the

structure of a molecule is negligibly small when phase transitions take place [32]. However, in some molecule-based materials, the change in the electronic state is strongly coupled with a change in the lattice. One such type occurs in transition-metal complexes with thermally driven transition between high- and low spin states, which is always accompanied by pronounced structural modifications originating from the different volume of the coordination polyhedron in the two states.

One of the main questions that emerged during the development of materials combining SCO and liquid crystalline properties was the reverse problem, *i.e.* can a structural phase transition of type Cr ↔ LC govern the spin crossover in a metallomesogen? It is possible to answer this question in part on the basis of the reported data dealing with the solid-state spin crossover materials. Among the nearly 200 reports on the spin crossover phenomenon cited in the ISI Web of Knowledge Data Base [34] over the last forty years nearly 40 describe synchronously occurring spin transition and phase transition with change of space group or disorder of the lattice components. As is now widely accepted, the occurrence of an independent or induced structural phase transition of the reconstructive type is not a prerequisite for the observation of the spin transition [27,35]. The structural transformation that compounds undergo during the spin transition by itself is a displacive phase transition which in favorable cases is efficient enough for the propagation of the cooperative interactions through the lattice and observation of all kinds of spin crossover transitions (abrupt, gradual, with hysteresis, *etc.*) [27]. In some cases, however, it can trigger the change of the space-group, but in general for systems where simultaneously spin- and structural transitions are observed the question about the primary effect arises, *i.e.* the structural phase transition induces the spin transition or vice versa leads to a "hen and egg" like problem. At least in some of the systems like those described in Refs. [36,37] the structural phase transition was determined not to be the driving force, but only the factor which modulates the character of the transition making it more steep up to the appearance of hysteresis which follows the structural transformation. Similarly, in the case of a very large hysteresis like in the systems $[Fe(PM\text{-}Pea)_2(NCS)_2]$, $[Fe(2\text{-}pic)_3]Cl_2{\cdot}H_2O$ a crystallographically significant phase transitions is held responsible for the spin transition [38,39]. For the rest of the systems the problem is seemingly unsolvable [37,38].

Another type of phase transition, namely the order–disorder phenomenon was discussed in the spin crossover literature since the report of Mikami et al. about the disorder of the solvent molecules in the spin transition complex $[Fe(2\text{-}pic)_3]Cl_2{\cdot}EtOH$ (2-pic = 2-(aminomethyl)pyridine) [40]. The structurally determined disorder of the ethanol molecule was suggested to trigger the two-step spin transition which later was confirmed in more precise studies [40,41]. Other types of disorder involve anions [42,43] and ligand moieties [43]. It was suggested that in these cases, the modification of the ligand field strength upon cooperative ordering of the lattice components provides an intrinsic impulse for the initiation of the spin crossover and observation of hysteresis loops or abrupt spin state change.

The phenomenon of polymorphism in spin crossover compounds also serves as convincing evidence of how important the character of the crystal packing, in particular the intermolecular contacts, for the spin crossover in the solid state is [39,44]. Changes of lattice vibrations as direct consequence of structural divergence are seemingly responsible factors governing different spin transition behaviour in different polymorphs. According to the variable temperature IR and Raman data supported by DFT calculation the distribution of the entropy gain in spin crossover iron(II) compounds is approximately as follows: nearly 27% is the share of the spin entropy, 40% is the contribution of the vibration-related entropy change mainly due to the metal-ligand skeletal vibrational modes and the rest of 33% is attributed to changes in lattice vibrations perturbed by intermolecular interactions [45]. The variation of the lattice indispensably changes the latter which leads to the change of the spin crossover properties.

Close interconnectivity of the phase transitions and the related macroscopic properties can also be found in molecular organic and metalorganic magnets where the change in the magnetic response is a measure of the inter- or intra-molecular interaction between paramagnetic centers. It intimately correlates with the adopted structure, therefore if the phase transition takes place, the magnetic properties follow the structural changes. Numerous examples also confirm that the reason for the observed anomalies in the magnetic susceptibility (or another property) of compounds possessing phase transitions is the modification of the relative disposition of the lattice components and therefore the degree of their interactions [46].

Also, examples of Co(II) coordination complexes incorporating alkyl chains where the valence-tautomerism [47] equilibrium is influenced by a solid–solid phase transition [48] and others exhibiting synchronicity between valence-tautomeric bistability and solid–melt phase transition have recently been reported [49].

Even knowing much about the paramount role of the intermolecular contacts in influencing properties of the bulk materials and the ability to modify them through phase transitions, does not help much the researchers to create new materials with required properties, in particular with the defined temperature of the transitions. All reported solid-state systems are more or less unique since they were mostly obtained sporadically. Thus the available experimental data have singular importance because they cannot be usually extended to create new even slightly modified systems. In this sense the use of the solid ↔ mesophase transitions instead of solid ↔ solid transitions is a more promising approach for the control of the structure-coupled properties in a new generation of the thermo-responsive molecular systems. The switching between the two states in such materials might be controlled by the melting temperature of the compound which in turn is defined by the easily controllable chemical structure. In the case of the metallomesogens the melting point depends on the length of the alkyl substituents. In the odd/even series of the homologous compounds, the temperature of the transition changes in a predictable way with lengthening of the alkyl chains [50].

Several examples of new iron(II)-based mononuclear and polymeric metallomesogens have been described in this review. Each compound was firstly examined in the non-alkylated form with the goal to determine the spin crossover properties excluding the influence of the alkoxy substituents [29,51]. Alkylation of the parent compounds caused appearance of the relatively low-temperature melting and mesomorphic properties [18–22]. In the following the reasons responsible for the observed influence of the phase transition on the magnetic properties of the alkylated compounds will be discussed.

In the solid state the ligand field strength of the spin crossover compounds is governed by a number of factors [12,13,27]. They can be divided into two groups. The first group includes those inherent variables which are defined by the chemical nature of the compound: type of the ligand, its substituents, type of the anion, crystal solvent and dimensionality. These are "inherent parameters" which cannot be changed by the external perturbation without degradation or irreversible chemical modification of the material. To the second group belong "structure-determined parameters". These are readily identifiable hydrogen bonds and π–π interactions which shape the pattern of the strong intermolecular contacts between the complex molecules. Other kinds of structure-dependent interactions include electrostatic and van der Waals types taken together as weak interactions. The structure-determined parameters can change in the course of a phase transition. The intermolecular

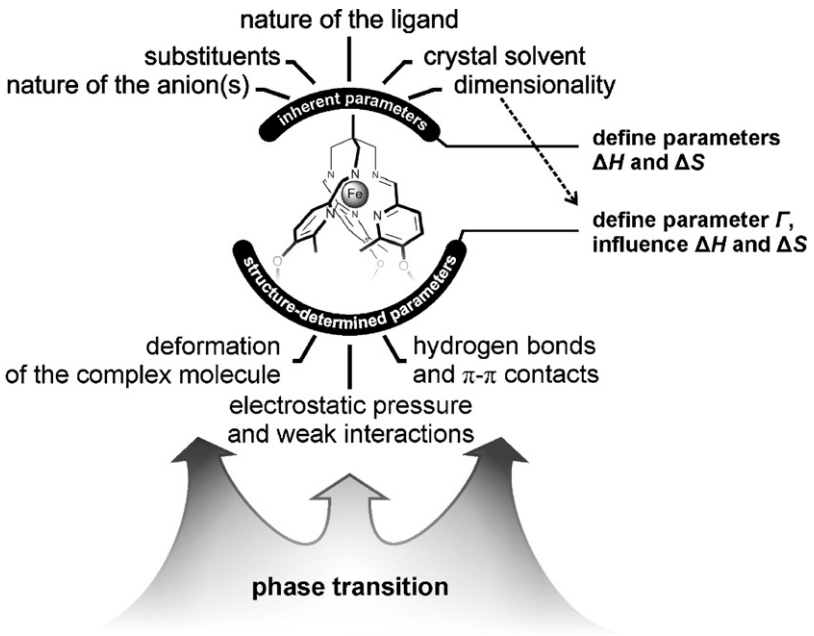

Fig. 15. Two subsets of parameters influencing the transition properties in spin crossover compounds. Phase transitions can modify only structure-determined parameters.

contacts modify the electronic structure of the ligand and transmit information about the spin state through the lattice. Any modification of these contacts, *e.g.* due to loss of solvent or phase transitions will lead to changes in the structure-dependent properties of the compound. One more source of the different behaviour in different phases is the structure-induced deformation of the complex molecule or of the ligand [51c]. The cumulative scheme of the parameters is depicted in Fig. 15.

Any kind of phase transition changing the patterns of the intermolecular contacts must be accompanied by the change in the character of the structure-related properties in spin crossover compounds. For example, the melting admittedly is accompanied by the decrease of the cooperativity. It is easy to imagine an increase of the volume during melting which means increase of distances between molecules and the following decrease of the contacts which mediate interactions between spin crossover centers. Therefore one can expect stabilization of the non-cooperative spin transition in the molten state and of the cooperative spin transition in the solid state. A change of the parameter Γ alone, corresponds to different cooperativity in two phases, whereas a concomitant change of the enthalpy ΔH and entropy ΔS would cause a difference in the critical temperature $T_{1/2}$ in the two phases, too.

Three types of interplay between spin crossover and solid → mesophase phase transitions have been indicated. The first one is type ia with coupled transitions. Members belonging to this group are the compounds $\mathbf{C_n}$**-1**·0.5H_2O where n = 16, 18 and 20 [18]. In these compounds before the phase transition Cr → S_A takes place, the magnetic susceptibility is insensitive to the variation of temperature, which means that the structure is of the type that blocks the spin transition below the melting point. This implies that the hypothetical temperature of the spin transition in the solid state $T_{1/2}{}^{solid}$ is much higher than the melting temperature (curve 1, Fig. 16a). Nevertheless, melting of the alkyl chains in these compounds modifies the structure in a way, that the molten samples show spin transition above the melting point. The reason for this is the pronounced change of the intermolecular contacts which is evident from the difference in thickness of the ionic bilayers of the liquid crystalline and solid samples determined from the XPRD data (the estimated value is *ca.* 6 Å). The amplitude of the structural transformation implies a change of all thermodynamical parameters, the cooperativity Γ, the entropy and enthalpy of the spin transition. In the molten state the cooperativity can approximate liquid-like behaviour which is typical for spin-equilibrium compounds (curve 2, Fig. 16a).

In the case of the compounds $\mathbf{C_n}$**-3** with n = 12, 14, 16 [19] the fitting of the magnetic curves before and after the phase transition sheds light on the changes which the systems undergo. As follows from the data, the melting decreases the parameter Γ that correlates with the moderate variation of the ionic bilayers due to the phase transition (the difference in the thickness is *ca.* 1 Å). Also the enthalpy and entropy are somewhat changed, which define inequality $T_{1/2}{}^{solid} < T_{1/2}{}^{mesophase}$. The spin-state change in $\mathbf{C_n}$**-3** induced by melting corresponds to the change from the more cooperative curve 3 to the less cooperative curve 4 (Fig. 16b). The superheating and supercooling on melting and solidification, respectively, cause the appearance of hysteresis of the structural transformation which is followed by the magnetic response.

The one-dimensional metallomesogens $\mathbf{C_n}$**-5** with n = 8, 10, 12 exhibit an incomplete thermally driven spin transition. A residual high spin fraction of *ca.* 50% is unusual and is due to the vitrification of the compounds, which provokes an inhibition of the spin transition process. This interplay between vitrification and SCO is analogous to the type ia) (curve 2, Fig. 16a), however, as expected in glass state there are no associated structural transformations.

The compounds $\mathbf{C_n}$**-6** with n = 10, 12 present similar mesomorphic behaviour as that observed for $MeC_6H_4SO_3^-$ derivatives, but they undergo complete thermal spin transition above 300 K accompanied by small hysteresis loops (Fig. 9a and b). In the compound $\mathbf{C_{12}}$**-6** the vitrification process was also found to modify the hysteresis loop making it asymmetric in comparison with the homologues with shorter alkyl chains. The change is less pronounced because of the small variation of the structure as is indicated by the variation of the interlayer distance *d*.

Conclusions can be drawn about the importance of the structural transformation due to the phase transition. The larger the variation of the structure, the more significant is the difference in the intermolecular contacts in the two phases and the more pronounced are differences in the properties of the molten system compared to the crystalline one. In the mononuclear systems the amplitude of the variation of the ionic bilayers is a measure of the structural transformation which leads to the modification of the spin crossover properties.

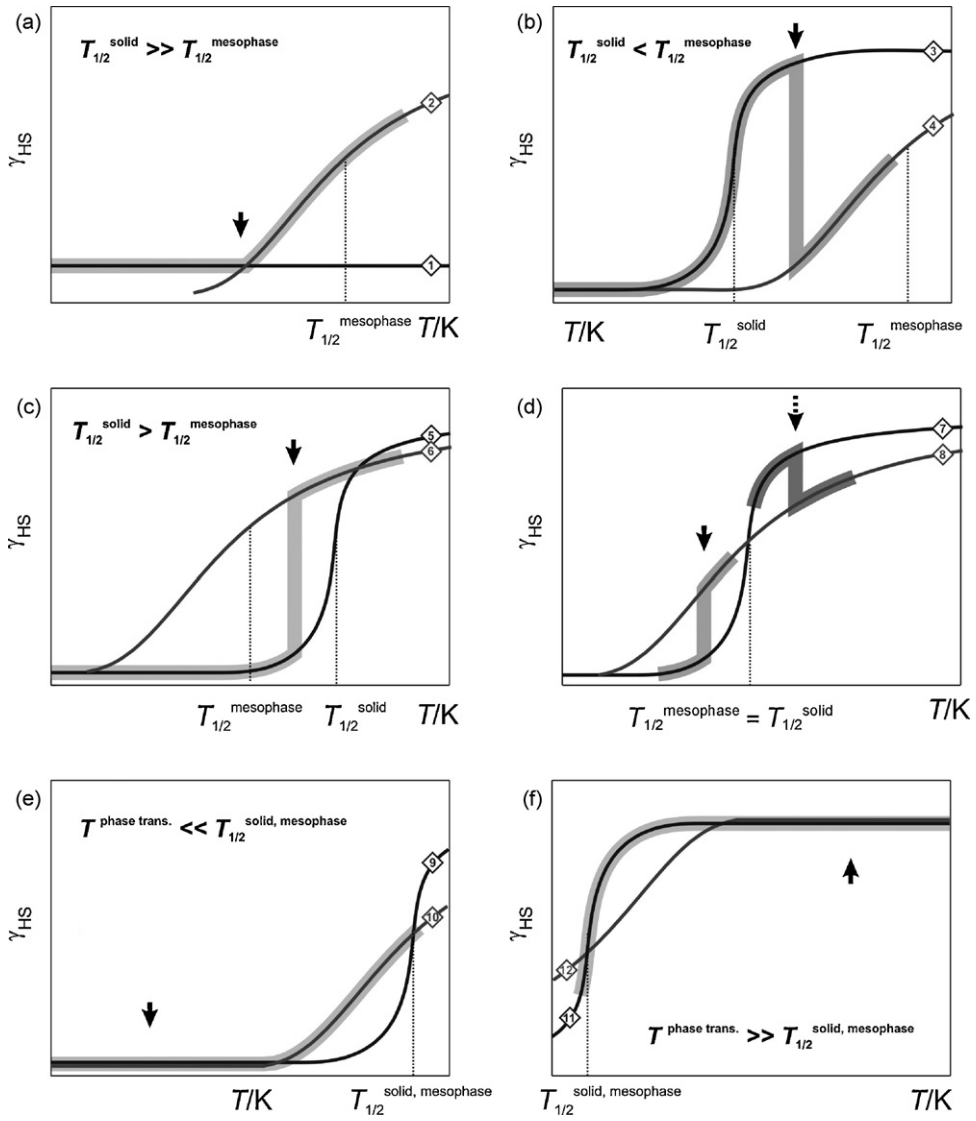

Fig. 16. Plots (a)–(f) illustrate transitions from solid-like behaviour (odd numbers) to the mesophase-like behaviour (even numbers). The bold curves show the resultant macroscopic responses with the abrupt change of the behaviour at the point of the phase transition (black bold arrow). The curves 1–12 were simulated using the Slichter–Drickamer model with different parameters of the enthalpy and entropy, which define the values $T_{1/2} = \Delta H/\Delta S$. The cooperativity parameters for the solid-state curves 1, 3, 5, 7, 9, 11 and for the mesophase curves 2, 4, 6, 8, 10, 12 obey the inequality $\Gamma^{solid} > \Gamma^{mesophase}$, *i.e.* in the mesophase spin transition is always less cooperative and therefore more gradual.

In systems of the type ii both the spin state change and the solid → mesophase transition coexist in the same temperature region but are not coupled. To these belong the compounds **C_n-1**·3.5H_2O, n = 16, 18, 20 and **C_n-5**·H_2O (n = 8, 10 and 12), which are insensitive to the melting, but not to the release of crystal water.

Worth to mention, that also two other possible types of the behaviour illustrated in Fig. 16c and d can be expected in spin crossover metallomesogens. The one which is characterized by inequality $T_{1/2}{}^{solid} > T_{1/2}{}^{mesophase}$ will lead to the behaviour similar to that of cooperative solid spin crossover compounds with the abrupt increase of the susceptibility in the melting point. A system where the phase transition causes a pronounced change of the cooperativity Γ and retains the parameter $T_{1/2}$ unchanged would manifest two different behaviours depending on the temperature at which the melting occurs.

The type iii is comprised by the systems where the two transitions are too far separated in temperature and therefore are not coupled. The spin transition can be located at relatively high temperatures resulting in low spin behaviour of the compound much above the melting temperature **C_{18}-2**: $T^{phase\ transition} \sim 380$ K, $T_{1/2}{}^{mesophase} \gg 400$ K) or can be located much lower in temperature (for example, **C_n-7** (n = 12 and 18): $T^{phase\ transition} \sim 380$ K, $T_{1/2}{}^{solid} = 133$ K). The first case is exemplified by curves 9 and 10 shown in Fig. 16e. Despite some possible modification of the intermolecular contacts and change of the curve from the solid-like curve 9 to the less cooperative mesophase-like curve 10, the transition temperature $T_{1/2}$ is still too high to cause any feasible changes in the magnetic response around the melting point. Similarly, the case of the low temperature spin crossover metallomesogens being insensitive to high-temperature phase transition is explained in Fig. 16f. The mononuclear iron(III) system reported by Galyametdinov et al. [15] and iron(II) systems reported by Hayami et al. [16,52] and [53], as well as polymeric one-dimensional systems investigated by Bodenthin et al. [54] also match type iii (Fig. 16e and f) since the independent spin transition and phase transition take place in different temperature regions.

We can conclude from the four archetypal transitions shown in Fig. 16a–d, that in order to observe the interplay of the phenomena it is necessary for the system to exhibit spin transition at least in one of the phases with the parameter $T_{1/2}$ located not far from the temperature of the solid → mesophase transition (Fig. 16a)

or inside the "loop" defined by the solid-like and mesophase-like curves (Fig. 16b–d).

6. Conclusion and perspectives

In this review article we have illustrated the strategies developed in order to achieve interplay/synergy between spin transition and liquid crystal transition. The synthesised Fe(II) metallomesogens exhibit different types of interplay between both phase transitions. A classification according to the analysis of the magnetic and structural data has led to the distinction of three types of interplay, namely:

Type i: systems with coupling between the electronic structure of the iron(II) ions and the mesomorphic behaviour of the substance.
Type ii: systems where both transitions coexist in the same temperature region but are not coupled due to competition with the dehydration.
Type iii: systems where both transitions occur in different temperature regions and therefore are uncoupled.

The future activity in the area of the spin crossover metallomesogens can be developed towards creation of new systems on the basis of the present results. Apart from the rich physical phenomenology observed in these materials the fact that spin crossover is accompanied by a pronounced change of colour, at least in Fe(II) metallomesogens, bears the promise for further technological applications in the liquid crystal field. In fact, we have demonstrated the possibility to prepare thermochomic liquid crystals operating in the room temperature region.

In our opinion, a promising next step in this research line is the development of photochromic liquid crystals by exploiting the possibility to induce spin state switching by ligand driven isomerization in analogy to the work of Zarembowitch and Boillot [55]. On the other hand, the ultimate goal in the area of spin crossover metallomesogens is the switching of the spin state utilizing the sensitivity of liquid crystalline phases to external electric and magnetic fields.

Acknowledgements

We acknowledge the financial support from the Deutsche Forschungsgemeinschaft (Priority Program 1137 "Molecular Magnetism") and the Fonds der Chemischen Industrie. A.B.G. thanks the Spanish MEC for a Ramon y Cajal research contract, for the project CTQ 2007-64727 and the Alexander von Humboldt Foundation for work-visiting fellowships. We are grateful to all people who have collaborated in this research project, V. Ksenofontov, Y. Galyametdinov, E. Rentschler, S. Reiman, W. Haase, Z. Tomkowicz, H. Ehrenberg, E. Welter, R. Dinnebier, E. Muth, P. Räder, J. Gutmann, M. Bach, S. Hess, B. Müller, J. Kusz, G. Bednarek, M. Verdaguer and F. Villain.

References

[1] (a) J.L. Serrano, Metallomesogens, VCH, Weinheim, 1996;
(b) S.A. Hudson, P.M. Maitlis, Chem. Rev. 93 (1993) 861;
(c) B. Donnio, D.W. Bruce, Struct. Bond. 95 (1999) 193;
(d) R.P. Lemieux, Acc. Chem. Res. 34 (2001) 845;
(e) R. Gimenez, D.R. Lydon, J.L. Serrano, Curr. Opin. Solid State Mater. Sci. 6 (2002) 527;
(f) J.L. Serrano, T. Sierra, Coord. Chem. Rev. 242 (2003) 73;
(g) B. Donnio, Curr. Opin. Colloid, Interface Sci. State Mater. Sci. 7 (2002) 371;
(h) D.W. Bruce, Acc. Chem. Res. 33 (2000) 831;
(i) C. Piguet, J.C.G. Bunzli, B. Donnio, D. Guillon, Chem. Commun. (2006) 3755.
[2] D. Vorländer, Ber. Dtsch. Chem. Ges. 43 (1910) 3120.
[3] A.M. Giroud, U.T. Müller-Westerhoff, Mol. Cryst. Liq. Cryst 41 (1977) 11.
[4] (a) Y. Galyametdinov, M.A. Athanassopoulou, K. Griesar, O. Kharitonova, E.A. Soto Bustamante, L. Tinchurina, I. Ovchinnikov, W. Haase, Chem. Mater. 8 (1996) 922;
(b) K. Binnemans, Y.G. Galyametdinov, R. Van Deun, D.W. Bruce, S.R. Collinson, A.P. Polishchuk, I. Bikchantaev, W. Haase, A.V. Prosvirin, L. Tinchurina, I. Litvinov, A. Gubajdullin, A. Rakhmatullin, K. Uytterhoeven, L. Van Meervelt, J. Am. Chem. Soc. 122 (2000) 4335;
(c) V.S. Mironov, Y.G. Galyametdinov, A. Ceulemans, C. Gorller-Walrand, K. Binnemans, J. Chem. Phys. 116 (2002) 4673.
[5] (a) Y.G. Galyametdinov, A.A. Knyazev, V.I. Dzhabarov, T. Cardinaels, K. Driesen, C. Görller-Walrand, K. Binnemans, Adv. Mater. 20 (2008) 252;
(b) V.N. Kozhevnikov, B. Donnio, D.W. Bruce, Angew. Chem., Int. Ed. Engl. 47 (2008) 6286.
[6] Z. Belarbi, C. Sirlin, J. Simon, J.J. Andre, J. Phys. Chem. 93 (1989) 8105.
[7] (a) D.W. Bruce, D.A. Dunmur, P.M. Maitlis, M.M. Manterfield, R. Orr, J. Mater. Chem. (1991) 255;
(b) D.W. Bruce, D.A. Dunmur, S.E. Hunt, P.M. Maitlis, R. Orr, J. Mater. Chem. 1 (1991) 857;
(c) G. Cipparrone, C. Versace, D. Duca, D. Pucci, M. Ghedini, C. Umcton, Mol. Cryst. Liq. Cryst. 212 (1992) 217.
[8] (a) B.A. Gregg, M.A. Fox, A.J. Bard, J. Phys. Chem. 94 (1990) 1586;
(b) M.J. Bacna, P. Espinet, M.B. Ros, J.L. Serrano, A. Ezcurra, Angew. Chem. Int. Ed. Eng. 32 (1993) 1203.
[9] (a) F.P. Shvartsman, V.A. Krongauz, Nature 309 (1984) 608;
(b) B.A. Gregg, M.A. Fox, A.J. Bard, J. Phys. Chem. 93 (1989) 4227;
(c) M. Irie, Chem. Rev. 100 (2000) 1683;
(d) M. Frigoli, G.H. Mehl, ChemPhysChem 4 (2003) 101;
(e) D.W. Bruce, P.A. Dunmur, M.A. Esteruelas, S.E. Hunt, P.M. Maitlis, J.R. Marsden, E. Sola, J.M. Stacey, J. Mater. Chem. 1 (1991) 251;
(f) M.A. Esteruelas, E. Sola, L.A. Oro, M.B. Ros, J.L. Serrano, Chem. Commun. (1986) 55;
(g) K. Ohta, H. Hasabe, M. Moriya, T. Fujimoto, I. Yamamoto, J. Mater. Chem. 1 (1991) 831;
(h) G. De Filpo, F.P. Nicoletta, G. Chidichimo, Adv. Mater. 17 (2005) 1150;
(i) M.P. Aldred, A.E.A. Contoret, S.R. Farrar, M.K. Stephen, D. Mathieson, M. O'Neill, W.C. Tsoi, P. Vlachos, Adv. Mater. 17 (2005) 1368.
[10] H.C. Chang, T. Shiozaki, A. Kamata, K. Kishida, T. Ohmori, D. Kiriya, T. Yamauchi, H. Furukawa, S. Kitagawa, J. Mater. Chem. 17 (2007) 4136.
[11] (a) P. Gütlich, G. Goodwin (Eds.), Top. Curr. Chem. vv. 233, 234, 235 (2004);
(b) A.B. Gaspar, V. Ksenofontov, M. Seredyuk, P. Gütlich, Coord. Chem. Rev 249 (2005) 2661;
(c) J.A. Real, A.B. Gaspar, V. Niel, M.C. Muñoz, Coord. Chem. Rev. 236 (2003) 121;
(d) Y. Garcia, P. Gütlich, Top. Curr. Chem. 234 (2004) 49.
[12] J.A. Real, A.B. Gaspar, M.C. Muñoz, Dalton Trans. (2005) 2062.
[13] P. Gütlich, A. Hauser, H. Spiering, Angew. Chem., Int. Ed. Engl. 33 (1994) 2024.
[14] (a) S. Decurtins, P. Gütlich, C.P. Köhler, H. Spiering, A. Hauser, Chem. Phys. Lett. 105 (1984) 1;
(b) J.F. Létard, J. Mater. Chem. 16 (2006) 2550.
[15] Y. Galyametdinov, V. Ksenofontov, A. Prosvirin, I. Ovchinnikov, G. Ivanova, P. Gütlich, W. Haase, Angew. Chem., Int. Ed. Engl. 40 (2001) 4269.
[16] (a) S. Hayami, K. Danjobara, K. Inoue, Y. Ogawa, N. Matsumoto, Y. Maeda, Adv. Mater. 16 (2004) 869;
(b) S. Hayami, N. Motokawa, A. Shuto, N. Masuhara, T. Someya, Y. Ogawa, K. Inoue, Y. Maeda, Inorg. Chem. 46 (2007) 1789.
[17] S. Hayami, R. Moriyama, A. Shuto, Y. Maeda, K. Ohta, K. Inoue, Inorg. Chem. 46 (2007) 7692.
[18] M. Seredyuk, A.B. Gaspar, V. Ksenofontov, Y. Galyametdinov, J. Kusz, P. Gütlich, J. Am. Chem. Soc. 130 (2008) 1431.
[19] M. Seredyuk, A.B. Gaspar, V. Ksenofontov, Y. Galyametdinov, J. Kusz, P. Gütlich, Adv. Funct. Mater. 18 (2008) 2089.
[20] M. Seredyuk, A.B. Gaspar, V. Ksenofontov, Y. Galyametdinov, M. Verdaguer, F. Villain, P. Gütlich, Inorg. Chem. 47 (2008) 10232.
[21] M. Seredyuk, A.B. Gaspar, V. Ksenofontov, S. Reiman, Y. Galyametdinov, W. Haase, E. Rentschler, P. Gütlich, Chem. Mater. 18 (2006) 2513.
[22] M. Seredyuk, A.B. Gaspar, V. Ksenofontov, S. Reiman, Y. Galyametdinov, W. Haase, E. Rentschler, P. Gütlich, Hyperfine Interact. 166 (2006) 385.
[23] T. Fujigaya, D.L. Jiang, T. Aida, J. Am. Chem. Soc. 125 (2003) 14690.
[24] D.L. Dorset, Crystallography of the Polymethylene Chain: An Inquiry into the Structure of Waxes, Oxford University Press, Oxford, New York, 2005.
[25] J.M. Seddon, in: D. Demus, J. Goodby, G.W. Gray, H.-W. Spiess, V. Vill (Eds.), Handbook of Liquid Crystals, vol. 1, Wiley-VCH, Weinheim, 1998, p. 635.
[26] (a) E.F. Marques, H.D. Burrows, M. da Miguel Graca, J. Chem. Soc., Faraday Trans. 94 (1998) 1729;
(b) C.G. Bazuin, D. Guillon, A. Skoulios, A.M. Amorim da Costa, H.D. Burrows, C.F.G.C. Geraldes, J.J.C. Teixeira-Dias, E. Blackmore, G.J.T. Tiddy, Liq. Cryst. 3 (1988) 1655.
[27] P. Gütlich, H.A. Goodwin, Top. Curr. Chem. 233 (2004) 1.
[28] C.P. Slichter, H.G. Drickamer, J. Chem. Phys. 56 (1972) 2142.
[29] M. Seredyuk, A.B. Gaspar, M.C. Munoz, M. Verdaguer, F. Villain, P. Gütlich, Eur. J. Inorg. Chem. (2007) 4481.
[30] A. Michalowicz, J. Moscovici, B. Ducourant, D. Cracco, O. Kahn, Chem. Mater. 7 (1995) 1833.
[31] (a) O. Kahn, J. Martinez, Science 279 (1998) 44;
(b) O. Roubeau, J.M.A. Gomez, E. Balskus, J.J.A. Kolnaar, J.G. Haasnoot, J. Reedijk, New J. Chem. 25 (2001) 144;
(c) C. Cantin, J. Kliava, A. Marbeuf, D. Mikaïlitchenko, Eur. Phys. J. B 12 (1999) 525.
[32] M. Sorai, Bull. Chem. Soc. Jpn. 74 (2001) 2223.
[33] C.N.R. Rao, K.J. Rao, Phase Transitions in Solids, McGraw-Hill, New York, 1978.

[34] http://isiknowledge.com.
[35] (a) L. Wiehl, G. Kiel, C.P. Köhler, H. Spiering, P. Gütlich, Inorg. Chem. 25 (1986) 1565;
(b) V. Petrouleas, J.P. Tuchagues, Chem. Phys. Lett. 137 (1987) 21;
(c) B. Gallois, J.A. Real, C. Hauw, J. Zarembowitch, Inorg. Chem. 29 (1990) 1152.
[36] (a) A.J. Conti, R.K. Chadha, K.M. Sena, A.L. Rheingold, D.N. Hendrickson, Inorg. Chem. 32 (1993) 2670;
(b) E. König, G. Ritter, S.K. Kulshreshtha, J. Waigel, L. Sacconi, Inorg. Chem. 23 (1984) 1241;
(c) C.C. Wu, J. Jung, P.K. Gantzel, P. Gütlich, D.N. Hendrickson, Inorg. Chem. 36 (1997) 5339.
[37] J. Kusz, P. Gütlich, H. Spiering, Top. Curr. Chem. 234 (2004) 129.
[38] P. Guionneau, M. Marchivie, G. Bravic, J.F. Létard, D. Chasseau, Top. Curr. Chem. 234 (2004) 97.
[39] P. Guionneau, J.F. Létard, D.S. Yufit, D. Chasseau, G. Bravic, A.E. Goeta, J.A.K. Howard, O. Kahn, J. Mater. Chem. 9 (1999) 985.
[40] M. Mikami, M. Konno, Y. Saito, Chem. Phys. Lett. 63 (1979) 566.
[41] (a) D. Chernyshov, M. Hostettler, K.W. Törnroos, H.B. Bürgi, Angew. Chem., Int. Ed. Engl. 42 (2003) 3825;
(b) D. Chernyshov, N. Klinduhov, K.W. Törnroos, M. Hostettler, B. Vangdal, H.B. Bürgi, Phys. Rev. B 76 (2007) 014406.
[42] (a) J. Fleisch, P. Gütlich, K.M. Hasselbach, W. Müller, Inorg. Chem. 15 (1976) 958;
(b) J.M. Holland, J.A. McAllister, Z.B. Lu, C.A. Kilner, M. Thornton-Pett, M.A. Halcrow, Chem. Commun. (2001) 577;
(c) V.A. Money, J. Elhaik, I.R. Evans, M.A. Halcrow, J.A.K. Howard, Dalton Trans. (2004) 65;
(d) E. König, G. Ritter, S.K. Kulshreshtha, S.M. Nelson, Inorg. Chem. 21 (1982) 3022.
[43] (a) G.S. Matouzenko, A. Bousseksou, S.A. Borshch, M. Perrin, S. Zein, L. Salmon, G. Molnar, S. Lecocq, Inorg. Chem. 43 (2004) 227;
(b) G.S. Matouzenko, D. Luneau, G. Molnar, N. Ould-Moussa, S. Zein, S.A. Borshch, A. Bousseksou, F. Averseng, Eur. J. Inorg. Chem. (2006) 2671.
[44] (a) A. Ozarowski, B.R. McGarvey, A.B. Sarkar, J.E. Drake, Inorg. Chem. 27 (1988) 628;
(b) G.S. Matouzenko, A. Bousseksou, S. Lecocq, P.J. van Koningsbruggen, M. Perrin, O. Kahn, A. Collet, Inorg. Chem. 36 (1997) 5869;
(c) M. Marchivie, P. Guionneau, J.F. Létard, D. Chasseau, Acta Crystallogr., Sect. B: Struct. Sci. 59 (2003) 479;
(d) A. Galet, A.B. Gaspar, M.C. Muñoz, G. Levchenko, J.A. Real, Inorg. Chem. 45 (2006) 9670.
[45] (a) A. Bousseksou, J.J. McGarvey, F. Varret, J.A. Real, J.P. Tuchagues, A.C. Dennis, M.L. Boillot, Chem. Phys. Lett. 318 (2000) 409;
(b) J.P. Tuchagues, A. Bousseksou, G. Molnar, J.J. McGarvey, F. Varret, Top. Curr. Chem. 235 (2004) 85.
[46] (a) A.J. Banister, N. Bricklebank, I. Lavender, J.M. Rawson, C.I. Gregory, B.K. Tanner, W. Clegg, M.R.J. Elsegood, F. Palacio, Angew. Chem., Int. Ed. Engl. 35 (1996) 2533;
(b) T.M. Barclay, A.W. Cordes, N.A. George, R.C. Haddon, M.E. Itkis, M.S. Mashuta, R.T. Oakley, G.W. Patenaude, R.W. Reed, J.F. Richardson, H. Zhang, J. Am. Chem. Soc. 120 (1998) 352;
(c) X. Ren, Q. Meng, Y. Song, C. Hu, C. Lu, X. Chen, Z. Xue, Inorg. Chem. 41 (2002) 5931;
(d) X. Ren, Q. Meng, Y. Song, C. Lu, C. Hu, Inorg. Chem. 41 (2002) 5686;
(e) J.L. Brusso, O.P. Clements, R.C. Haddon, M.E. Itkis, A.A. Leitch, R.T. Oakley, R.W. Reed, J.F. Richardson, J. Am. Chem. Soc. 126 (2004) 14692;
(f) J.L. Brusso, O.P. Clements, R.C. Haddon, M.E. Itkis, A.A. Leitch, R.T. Oakley, R.W. Reed, J.F. Richardson, J. Am. Chem. Soc. 126 (2004) 8256;
(g) X.M. Ren, H. Okudera, R.K. Kremer, Y. Song, C. He, Q.J. Meng, P.H. Wu, Inorg. Chem. 43 (2004) 2569;
(h) A. Alberola, R.J. Collis, S.M. Humphrey, R.J. Less, J.M. Rawson, Inorg. Chem. 45 (2006) 1903;
(i) W. Fujita, K. Awaga, R. Kondo, S. Kagoshima, J. Am. Chem. Soc. 128 (2006) 6016;
(j) X.M. Ren, S. Nishihara, T. Akutagawa, S. Noro, T. Nakamura, Inorg. Chem. 45 (2006) 2229.
[47] D.N. Hendrickson, C.G. Pierpont, Top. Curr. Chem. 234 (2004) 63.
[48] D. Kiriya, H.-C. Chang, A. Kamata, S. Kitagawa, Dalton Trans. (2006) 1377.
[49] D. Kiriya, H.-C. Chang, S. Kitagawa, J. Am. Chem. Soc. 130 (2008) 5515.
[50] A.I. Kitaigorodski, Organic Chemical Crystallography, Consultants Bureau, New York, 1961.
[51] (a) G. Brewer, C. Luckett, L. May, A.M. Beatty, W.R. Scheidt, Inorg. Chim. Acta 357 (2004) 2390;
(b) M. Seredyuk, A.B. Gaspar, J. Kusz, G. Bednarek, P. Gütlich, J. Appl. Crystallogr. 40 (2007) 1135;
(c) M. Seredyuk, Ph.D. Thesis, University of Mainz, 2008.
[52] S. Hayami, K. Danjobara, S. Miyazaki, K. Inoue, Y. Ogawa, Y. Maeda, Polyhedron 24 (2005) 2821.
[53] S. Hayami, N. Motokawa, A. Shuto, R. Moriyama, N. Masuhara, K. Inoue, Y. Maeda, Polyhedron 26 (2007) 2375.
[54] Y. Bodenthin, U. Pietsch, H. Mohwald, D.G. Kurth, J. Am. Chem. Soc. 127 (2005) 3110.
[55] (a) J. Zarembowitch, C. Roux, M.L. Boillot, R. Claude, J.P. Itie, A. Polian, M. Bolte, Mol. Cryst. Liq. Cryst. 234 (1993) 247;
(b) C. Roux, J. Zarembowitch, B. Gallois, T. Granier, R. Claude, Inorg. Chem. 33 (1994) 2273;
(c) M.L. Boillot, A. Sour, P. Delhaes, C. Mingotaud, H. Soyer, Coord. Chem. Rev. 192 (1999) 47;
(d) M.L. Boillot, J. Zarembowitch, A. Sour, Top. Curr. Chem. 234 (2004) 261.